

Certification of genuine multipartite entanglement in spin ensembles with measurements of total angular momentum

Khoi-Nguyen Huynh-Vu,¹ Lin Htoo Zaw,² and Valerio Scarani^{2,3}

¹*College of Engineering and Computer Science, VinUniversity, Gia Lam district, Hanoi 14000, Vietnam*
²*Centre for Quantum Technologies, National University of Singapore, 3 Science Drive 2, Singapore 117543*
³*Department of Physics, National University of Singapore, 2 Science Drive 3, Singapore 117542*

We introduce entanglement witnesses for spin ensembles which detect genuine multipartite entanglement using only measurements of the total angular momentum. States that are missed by most other angular-momentum-based witnesses for spin ensembles, which include Greenberger-Horne-Zeilinger states and certain superpositions of Dicke states, can be effectively detected by our witness. The protocol involves estimating the probability that the total angular momentum is positive along equally-spaced directions on a plane. Alternatively, one could measure along a single direction at different times, under the assumption that the total spins undergo a uniform precession. Genuine multipartite entanglement is detected when the observed score exceeds a separable bound. Exact analytical expressions for the separable bound are obtained for spin ensembles $j_1 \otimes j_2 \otimes \dots \otimes j_N$ such that the total spin is a half-integer, and numerical results are reported for the other cases. Finally, we conjecture an expression for the separable bound when the total spin is not known, which is well supported by the numerical results.

I. INTRODUCTION

Entanglement is an important resource that enables many quantum protocols [1–3]. For this reason, the experimental certification of entanglement in real quantum devices is extremely important for both practical and foundational purposes. Consequently, many methods for detecting entanglement have been proposed and studied since the early days of quantum information [4]. Entanglement witnesses can be constructed analytically or numerically [5, 6], and it is even possible to certify entanglement without full characterization of the measurement device [7, 8].

However, there are some challenges when implementing entanglement witnesses in practice. Each experimental setup has measurements and operations that are native to that system. In general, arbitrarily constructed witnesses would require measurements in bases different from the native ones. So, some operations on the state need to be performed prior to measurement, which impacts the fidelity of the measurement. Alternatively, full or partial tomography must be done to extract the expectation value of the witness from the tomographic data, but tomography can be intractable for large systems. As such, when taking pragmatic reasons into account, witnesses that depend only on measurements native to the experimental setup might be more suitable in some cases.

In this paper, we focus on the *spin ensemble*, a collection of particles labeled by n , each with a fixed spin j_n . Experimental settings in which spin ensembles appear include ultracold atoms in optical lattices [9], and spin defects [10] and donors [11] in solid state materials. Measurements of angular momentum $\vec{J}^{(j_n)}$ are natural in such systems. We take that any component (e.g. J_x) or function of \vec{J} (e.g. $|\vec{J}|^2$) can be easily measured.

Several novel witnesses that utilize only angular momentum measurements have been introduced for spin en-

sembles. A mainstay are the spin-squeezing inequalities [1, 12, 13], which are based on variances of different angular momentum components, and are built upon the uncertainty relations of spin observables. Following the seminal paper by Sørensen *et al.* [14], generalized spin-squeezing criteria have also been proposed to detect the entanglement of two to three spin-half particles [15, 16], approximate many-body singlet states [17], and symmetric Dicke states [18]. Families of such multipartite witnesses have also been characterized for spin-half particles [19, 20], and later, for more general spin ensembles [21, 22].

Another notable approach involves the energy observable, which, for spin ensembles, are some function of the angular momentum operators [23]. If the ground state of the Hamiltonian is known to be entangled, and the measured energy is below a certain threshold, then the system itself must be entangled. Energy-based witnesses have been applied to various spin models, including XY [24–26], XYZ [27], Heisenberg [24], and more general spin chains [28–30].

Since these witnesses act upon spin ensembles, the witnessed correlations are that of entanglement between many particles. Such multipartite entanglement takes on a more complex character in comparison to bipartite entanglement. First, the entanglement might be dependent on the partition chosen: For example, $\propto (|\uparrow\downarrow\rangle_{1,2} - |\downarrow\uparrow\rangle_{1,2}) \otimes |\downarrow\rangle_3$ is entangled over the $\{1\}-\{2,3\}$ partition, but separable over the $\{1,2\}-\{3\}$ partition. As such, the stronger notion of *genuine multipartite entanglement* (GME) has to be introduced: The entanglement present in a state is defined to be GME if it *cannot* be written as a convex combination of separable states, where the separability of each state can be over *any* bipartition [31]. Second, there are inequivalent types of maximally entangled states that cannot be interconverted using only local operations and classical commu-

nication: For three spin-half particles, these are the W state $|W_3\rangle \propto |\uparrow\downarrow\downarrow\rangle + |\downarrow\uparrow\downarrow\rangle + |\downarrow\downarrow\uparrow\rangle$ and the Greenberger-Horne-Zeilinger (GHZ) state $|\text{GHZ}_3\rangle \propto |\uparrow\rangle^{\otimes 3} + |\downarrow\rangle^{\otimes 3}$ [32].

In terms of the different types of multipartite entanglement, only some of the aforementioned angular-momentum-based witnesses can detect GME [25, 33–36], and those that do are mostly effective at detecting Dicke states [37], a generalization of W states. Notably missing are angular-momentum-based witnesses that can detect N -partite GHZ states $|\text{GHZ}_N\rangle \propto |\uparrow\rangle^{\otimes N} + |\downarrow\rangle^{\otimes N}$ beyond the tripartite case. Since GHZ states are resources for distributed computing [38], and are also useful in quantum secret sharing protocols [39], angular-momentum-based witnesses that can detect GHZ states are desirable.

The primary contribution of this paper is to fill this gap. We introduce a witness of GME that requires only measurements of the total angular momentum of the spin ensemble, and can detect states that are missed by existing angular-momentum-based criteria, in particular, our witness can detect N -partite GHZ states.

II. THE PRECESSION PROTOCOL

A. The Protocol as a nonclassicality test

We first present the protocol as a nonclassicality test. It consists of many independent rounds. In each round, one system is prepared in some state, then its total angular momentum is measured along one of the directions

$$\begin{aligned} J_k &:= e^{-i(2\pi k/K)J_z/\hbar} J_x e^{i(2\pi k/K)J_z/\hbar} \\ &= \cos(2\pi k/K)J_x + \sin(2\pi k/K)J_y, \end{aligned} \quad (1)$$

where $k \in \{0, 1, \dots, K-1\}$, K is a positive integer, and where the x - y plane of the measurement directions can be chosen at one's convenience. After many such rounds, the average probability that J_k was found to be positive is calculated as the score

$$P_K := \frac{1}{K} \sum_{k=0}^{K-1} \left[\Pr(J_k > 0) + \frac{1}{2} \Pr(J_k = 0) \right]. \quad (2)$$

The protocol does not specify, as conditions for its validity, that the state be the same in each round (of course, if the preparation is not under good control, the score will be low); nor does it matter that the measurement k be chosen in any particular order or at random. However, the preparation of the state and the choice of direction k for the measurement must be uncorrelated (we could say that “the measurement should be random, i.e., unpredictable, from the point of view of the system”).

This protocol is based on a test known as the “precession protocol” or “Tsirelson protocol” [40–42], which is a witness of nonclassicality for single systems. The first expression comes from a dynamical assumption in those works that we do not use here (see Sec. II C 2); however,

for the sake of a name, we shall continue to refer to this protocol as to *the precession protocol*.

The upper bound $P_K \leq \mathbf{P}_K^c$ predicted by classical theory is $\mathbf{P}_K^c = 1/2$ for K even and $\mathbf{P}_K^c = (1+1/K)/2$ for K odd [40, 41]. Meanwhile, the expected score for a quantum system in the state ρ is given by $P_K = \text{tr}(\rho Q_K)$, with

$$Q_K := \frac{1}{K} \sum_{k=0}^{K-1} \text{pos}(J_k). \quad (3)$$

Here, $\text{pos}(J_k)$ is defined on the eigenstates $|j, m\rangle_k$ of J_k , such that $J_k |j, m\rangle_k = \hbar m |j, m\rangle_k$ and $2 \text{pos}(J_k) |j, m\rangle_k = [1 + \text{sgn}(m)] |j, m\rangle_k$, with the usual convention $\text{sgn}(0) = 0$. There exist quantum states that violate the classical bound. In particular, the maximal eigenstates of Q_K (the states that achieve the largest quantum score) are known in some cases [41]. Therefore, upon performing the protocol, the observation $P_K > \mathbf{P}_K^c$ detects the nonclassicality of the measured system.

B. Protocol as an entanglement witness

We will now apply the precession protocol to the total angular momentum \vec{J} of a composite system. Concretely, let us consider a spin ensemble consisting of N particles with fixed spins j_1, j_2, \dots, j_N . With a slight abuse of notation, the angular momentum along the k direction of the n th spin is denoted by

$$J_k^{(j_n)} = \mathbb{1}^{(j_1)} \otimes \dots \otimes \mathbb{1}^{(j_{n-1})} \otimes J_k^{(j_n)} \otimes \mathbb{1}^{(j_{n+1})} \otimes \dots \otimes \mathbb{1}^{(j_N)}, \quad (4)$$

such that $J_k^{(j)}$ for a fixed spin is given by

$$J_k^{(j)} = \sum_{m=-j}^j \hbar m |j, m\rangle_k \langle j, m|, \quad (5)$$

where $|j, m\rangle_k$ is a simultaneous eigenstate of $|\vec{J}|^2$ and J_k with eigenvalues $\hbar^2 j(j+1)$ and $\hbar m$ respectively. It is related to the usual eigenstate $|j, m\rangle$ of $|\vec{J}|^2$ and J_z by $|j, m\rangle_k = e^{-i(2\pi k/K)J_z/\hbar} e^{-i(\pi/2)J_y/\hbar} |j, m\rangle$.

With this, we can consider an implementation of the precession protocol with $J_k = \sum_{n=1}^N J_k^{(j_n)}$, and ask whether a composite system performs better in this protocol when the particles are entangled, in other words, whether we can define a *precession-based entanglement witness (PEW)*. Previous works suggest it to be so: for two fixed spins, the state conjectured to be maximally violating is always entangled [41]; for two harmonic oscillators, violation by a linear combination of the original modes implies entanglement of the latter in a wide parameter range [43].

Indeed, we shall show that a sufficiently large violation of the classical bound by the spin ensemble implies GME. Our main results are as follows: an exact analytical bound when $\sum_{n=1}^N j_n = K/2$, for all odd $K \geq 3$

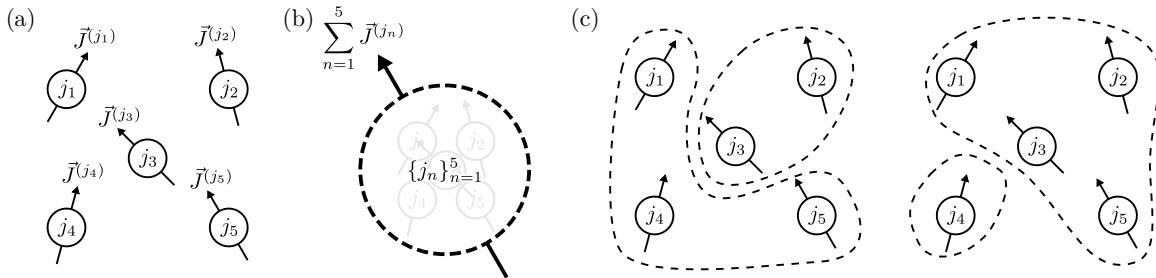


FIG. 1. (a) We consider a spin ensemble of N particles. Each particle has a fixed spin j_n with angular momentum $\vec{J}^{(j_n)}$. (b) The protocol is performed on the total angular momentum $\vec{J} = \sum_{n=1}^N \vec{J}^{(j_n)}$ of the spin ensemble $\{j_n\}_{n=1}^N$, which is the sum of the individual angular momentum of each particle. (c) In general, the entanglement of a spin ensemble depends on how the ensemble is partitioned. The system might be entangled over one bipartition, but separable over another. As such, we are interested in the stronger notion of *genuine multipartite entanglement* (GME): a state is GME if it cannot be written as a mixture of separable states, where the separability of the state can be over *any* bipartition. Our entanglement witness detects GME if the score of the precession protocol is found to be larger than a separable bound.

(Result 1); and a conjectured bound for all cases (Conjecture 3), with strong numerical evidence for $\sum_{n=1}^N j_n \leq 15$ and $K \leq 21$ (Result 4).

C. Remarks on the implementation of the protocol

1. Collective measurements are possible but not necessary

Our PEW belongs to the class of *angular-momentum-based entanglement witnesses*. Indeed, it can be implemented by measuring only collective observables, namely, the suitable components of the total \vec{J} .

That being said, collective measurements are not necessary. Because $J_k = \sum_{n=1}^N J_k^{(j_n)}$, any measurement of J_k can be done by first locally measuring $J_k^{(j_n)}$ for each spin, or $\sum_{n \in \{n_1, n_2, \dots\}} J_k^{(j_n)}$ for a subset of spins; then manually adding up the measurement outcomes afterwards. This feature is shared with some other witnesses [18, 24], but is contrasted with those that require measurements in a nonlocal basis [17].

2. Measuring along only one direction under the assumption of dynamics

In the earlier works about the precession protocol as a nonclassicality test [40–42], the protocol was presented as a measurement of a single observable at different times, under the assumption that, during the certification process, that observable undergoes a uniform precession. Specifically, if $\vec{J} = (J_x, J_y, J_z)$ is known to precess uniformly about the z axis with period $T := 2\pi/\omega$ as

$$\vec{J}(t) = \begin{pmatrix} \cos(\omega t)J_x(0) + \sin(\omega t)J_y(0) \\ \cos(\omega t)J_y(0) - \sin(\omega t)J_x(0) \\ J_z(0) \end{pmatrix}, \quad (6)$$

then indeed $J_k(0) = J_x(t_k)$ for $t_k = (k/K)T$. In this dynamical implementation, upon drawing k , one would wait until time t_k and then measure J_x . In some systems, having to measure only in one direction could be an advantage, coming at the cost of the assumption on the dynamics. Hence, this offers another way of performing the precession protocol, rather than measuring at a fixed time along one among several directions as we present in this paper.

This alternate method can be useful in witnessing the entanglement of postquench states, which is a common problem in the study of spin ensembles [26, 44]. Here, “*quenching*” refers to a sudden change of some parameters of the Hamiltonian. By starting with a highly entangling Hamiltonian, then quenching to the free Hamiltonian $H = -\omega J_z$, the dynamical assumption of uniform precession holds, and the precession protocol can be performed.

This approach fits naturally with recent efforts in optimal quantum control that seeks to engineer driven Hamiltonians that achieve target states with GME, like the GHZ state [45, 46]. Our protocol provides a way to certify the success of the quantum control procedure after it has been implemented.

III. MAIN RESULTS: SEPARABLE BOUNDS

In this section, we detail the results with which we will eventually arrive at Results 1 and 4 and Conjecture 3.

Since we are interested in detecting GME states, we have to consider *every possible bipartition* of the spin ensemble, as illustrated in Fig. 1. Let us therefore formalize the notion of a bipartition of a spin ensemble $\{j_n\}_{n=1}^N$. When partitioning the spin ensemble into two subsets, if the first subset is $\mathbf{J} = \{j_{n_1}, j_{n_2}, \dots, j_{n_L}\}$ containing $1 \leq L < N$ spins, then the second subset will contain the remaining spins $\mathbf{J}^c := \{j_n\}_{n=1}^N \setminus \mathbf{J}$. Meanwhile, for all possible bipartitions, the first subset can be any

$\mathbf{J} \in 2^{\{j_n\}_{n=1}^N} \setminus \{\emptyset, \{j_n\}_{n=1}^N\}$, where $2^{\{j_n\}_{n=1}^N}$ is the power set of $\{j_n\}_{n=1}^N$, and we exclude \emptyset and its complement to ensure that at least one spin is present in each partition.

In addition, $\mathcal{H}^{(j_n)}$ denotes the Hilbert space spanned by $\{|j_n, m\rangle\}_{m=-j_n}^{j_n}$. We will also loosely call both $\sum_m \psi_m |j_n, m\rangle$ and $\sum_{m, m'} \rho_{m, m'} |j_n, m\rangle \langle j_n, m'| \geq 0$, pure and mixed states, respectively, as “states that belong in $\mathcal{H}^{(j_n)}$ ”.

With these notations, a state $\rho_{\mathbf{J}, \mathbf{J}^c}$ of a spin ensemble is separable over the $\mathbf{J}-\mathbf{J}^c$ bipartition if $\rho_{\mathbf{J}, \mathbf{J}^c} = \sum_k p_k \rho_{\mathbf{J}, k} \otimes \rho_{\mathbf{J}^c, k}$, where $\rho_{\mathbf{J}, k}$ (or $\rho_{\mathbf{J}^c, k}$) is a state within the subspace $\bigotimes_{j \in \mathbf{J}} \mathcal{H}^{(j)}$ (or $\bigotimes_{j' \in \mathbf{J}^c} \mathcal{H}^{(j')}$). Conversely, ρ_{GME} is GME if it is not a convex combination of states separable over any bipartition \mathbf{J} : that is, $\rho_{\text{GME}} \neq \sum_{\mathbf{J}} p_{\mathbf{J}} \rho_{\mathbf{J}, \mathbf{J}^c}$.

Finally, we define the separable bound $\mathbf{P}_K^{\text{sep}}(\{j_n\}_{n=1}^N)$ as the maximum score achieved by a non-GME state of the spin ensemble $\{j_n\}_{n=1}^N$, upon performing the precession protocol on the total angular momentum of the spin ensemble:

$$\begin{aligned} \mathbf{P}_K^{\text{sep}}(\{j_n\}_{n=1}^N) &:= \max_{\{\rho_{\mathbf{J}, \mathbf{J}^c}\}} \text{tr} \left[\left(\sum_{\mathbf{J}} p_{\mathbf{J}} \rho_{\mathbf{J}, \mathbf{J}^c} \right) Q_K \right] \\ &= \max_{\mathbf{J}} \max_{\rho_{\mathbf{J}, \mathbf{J}^c}} \text{tr}(\rho_{\mathbf{J}, \mathbf{J}^c} Q_K). \end{aligned} \quad (7)$$

Here, convexity was used in the first line, Q_K is as defined in Eq. (3) with $\vec{J} = \sum_{n=1}^N \vec{J}^{(j_n)}$, while the maximizations are over all $\mathbf{J} \in 2^{\{j_n\}_{n=1}^N} \setminus \{\emptyset, \{j_n\}_{n=1}^N\}$ and $\rho_{\mathbf{J}, \mathbf{J}^c} = \sum_k p_k \rho_{\mathbf{J}, k} \otimes \rho_{\mathbf{J}^c, k}$, where $\mathbf{J}^c = 2^{\{j_n\}_{n=1}^N} \setminus \mathbf{J}$.

By definition, every non-GME state must achieve the score $P_K \leq \mathbf{P}_K^{\text{sep}}(\{j_n\}_{n=1}^N)$. The negation of this statement implies that if the separable bound is violated, the system must be GME. Therefore, our PEW detects GME states if the score $P_K > \mathbf{P}_K^{\text{sep}}(\{j_n\}_{n=1}^N)$ is achieved when performing the precession protocol on the total angular momentum of the spin ensemble $\{j_n\}_{n=1}^N$.

A. Relation between the multipartite and bipartite separable bounds

By taking advantage of the decomposition of Q_K in terms of the irreducible blocks of the angular momentum observable, the separable bounds of large spin ensembles can be related to separable bounds of two-spin systems.

For a particular bipartition $\mathbf{J} := \{j_{n_l}\}_{l=1}^L$, the usual rules for the addition of angular momentum applied to the total angular momentum $\vec{J} = \sum_{n=1}^N \vec{J}^{(j_n)}$ results in

the decomposition [47]

$$\begin{aligned} \vec{J} &= \sum_{l=1}^L \vec{J}^{(j_{n_l})} + \sum_{l'=L+1}^N \vec{J}^{(j_{n_{l'}})} \\ &= \bigoplus_{\substack{j_1=j_1+j_2 \\ \tilde{j}_1=|j_{n_1}-j_{n_2}|}} \bigoplus_{\substack{j_2=j_2+j_3 \\ \tilde{j}_2=|\tilde{j}_1-j_{n_3}|}} \cdots \bigoplus_{\substack{j_{L-2}=j_{L-2}+j_{n_L} \\ \tilde{j}=|\tilde{j}_{L-2}-j_{n_L}|}} \vec{J}^{(\tilde{j})} \\ &\quad + \bigoplus_{\substack{j_{L+1}=j_{L+1}+j_{n_{L+2}} \\ \tilde{j}'_1=|j_{n_{L+1}}-j_{n_{L+2}}|}} \cdots \bigoplus_{\substack{j_{N-L-2}=j_{N-L-2}+j_{n_N} \\ \tilde{j}'=|\tilde{j}'_{N-L-2}-j_{n_N}|}} \vec{J}^{(\tilde{j}')}, \\ &=: \bigoplus_{\tilde{j} \in \mathcal{J}(\mathbf{J})} \bigoplus_{\tilde{j}' \in \mathcal{J}(\mathbf{J}^c)} \left[\vec{J}^{(\tilde{j})} \otimes \mathbb{1}^{(\tilde{j}')} + \mathbb{1}^{(\tilde{j})} \otimes \vec{J}^{(\tilde{j}')} \right], \end{aligned} \quad (8)$$

where $\mathcal{J}(\{j_{n_1}, j_{n_2}, \dots, j_{n_L}\}) := \{\tilde{j} : |\tilde{j}_{L-2} - j_{n_L}| \leq \tilde{j} \leq \tilde{j}_{L-2} + j_{n_L}, |\tilde{j}_{L-3} - j_{n_{L-1}}| \leq \tilde{j}_{L-2} \leq \tilde{j}_{L-3} + j_{n_{L-1}}, \dots, |j_{n_1} - j_{n_2}| \leq \tilde{j}_1 \leq j_{n_1} + j_{n_2}\}$ is the set of irreducible spins of the block decomposition of $\sum_{l=1}^L \vec{J}^{(j_{n_l})}$, which does not depend on the order of the elements of $\{j_{n_l}\}_{l=1}^L$ in its definition. The implicit tensor product with the identity has been made visible in Eq. (8), which makes explicit that each term in the square brackets has nonzero support only in the $\mathcal{H}^{(\tilde{j})} \otimes \mathcal{H}^{(\tilde{j}')}$ subspace.

It follows that, for an observable $f(\vec{J})$ that is a function of the total angular momentum,

$$\begin{aligned} &\text{tr} \left[\rho_{\mathbf{J}, \mathbf{J}^c} f(\vec{J}) \right] \\ &= \sum_{\substack{\tilde{j} \in \mathcal{J}(\mathbf{J}), \\ \tilde{j}' \in \mathcal{J}(\mathbf{J}^c)}} \text{tr} \left[\rho_{\mathbf{J}, \mathbf{J}^c} f \left(\mathbb{1}^{(\tilde{j})} \otimes \vec{J}^{(\tilde{j}')} + \vec{J}^{(\tilde{j})} \otimes \mathbb{1}^{(\tilde{j}')} \right) \right]. \end{aligned} \quad (9)$$

In addition, using the convexity of the set $\{\rho_{\mathbf{J}, \mathbf{J}^c}\}$,

$$\max_{\rho_{\mathbf{J}, \mathbf{J}^c}} \text{tr} \left[\rho_{\mathbf{J}, \mathbf{J}^c} f(\vec{J}) \right] = \max_{|\Psi_{\mathbf{J}}, \Psi_{\mathbf{J}^c}\rangle} \langle \Psi_{\mathbf{J}}, \Psi_{\mathbf{J}^c} | f(\vec{J}) | \Psi_{\mathbf{J}}, \Psi_{\mathbf{J}^c} \rangle, \quad (10)$$

where the maximization is over $|\Psi_{\mathbf{J}}, \Psi_{\mathbf{J}^c}\rangle = |\Psi_{\mathbf{J}}\rangle \otimes |\Psi_{\mathbf{J}^c}\rangle$, with $|\Psi_{\mathbf{J}}\rangle \in \bigotimes_{j \in \mathbf{J}} \mathcal{H}^{(j)}$ and $|\Psi_{\mathbf{J}^c}\rangle \in \bigotimes_{j' \in \mathbf{J}^c} \mathcal{H}^{(j')}$, which are pure states separable over the $\mathbf{J}-\mathbf{J}^c$ bipartition.

In relation to $\bigotimes_{j \in \mathbf{J}} \mathcal{H}^{(j)} = \bigoplus_{\tilde{j} \in \mathcal{J}(\mathbf{J})} \mathcal{H}^{(\tilde{j})}$, $|\Psi_{\mathbf{J}}\rangle$ can be rewritten as $|\Psi_{\mathbf{J}}\rangle = \bigoplus_{\tilde{j} \in \mathcal{J}(\mathbf{J})} \sqrt{p_{\tilde{j}}} |\psi_{\tilde{j}}\rangle$ with independent parameters $\vec{p} = (p_{\tilde{j}})_{\tilde{j} \in \mathcal{J}(\mathbf{J})}$ and $\{|\psi_{\tilde{j}}\rangle\}_{\tilde{j} \in \mathcal{J}(\mathbf{J})}$, where $0 \leq p_{\tilde{j}} \leq 1$, $\sum_{\tilde{j} \in \mathcal{J}(\mathbf{J})} p_{\tilde{j}} = 1$, and $|\psi_{\tilde{j}}\rangle \in \mathcal{H}^{(\tilde{j})}$.

Similarly with $|\Psi_{\mathbf{J}^c}\rangle = \bigoplus_{\tilde{j}' \in \mathcal{J}(\mathbf{J}^c)} \sqrt{p'_{\tilde{j}'}} |\psi_{\tilde{j}'}\rangle$, we have

$$|\Psi_{\mathbf{J}}, \Psi_{\mathbf{J}^c}\rangle = \bigoplus_{\substack{\tilde{j} \in \mathcal{J}(\mathbf{J}), \\ \tilde{j}' \in \mathcal{J}(\mathbf{J}^c)}} \sqrt{p_{\tilde{j}} p'_{\tilde{j}'}} |\psi_{\tilde{j}}, \psi_{\tilde{j}'}\rangle, \quad (11)$$

where $|\psi_{\tilde{j}}, \psi_{\tilde{j}'}\rangle = |\psi_{\tilde{j}}\rangle \otimes |\psi_{\tilde{j}'}\rangle$. Therefore,

$$\begin{aligned} &\langle \Psi_{\mathbf{J}}, \Psi_{\mathbf{J}^c} | f \left(\mathbb{1}^{(\tilde{j})} \otimes \vec{J}^{(\tilde{j}')} + \vec{J}^{(\tilde{j})} \otimes \mathbb{1}^{(\tilde{j}')} \right) | \Psi_{\mathbf{J}}, \Psi_{\mathbf{J}^c} \rangle \\ &= p_{\tilde{j}} p'_{\tilde{j}'} \langle \psi_{\tilde{j}}, \psi_{\tilde{j}'} | f \left(\mathbb{1}^{(\tilde{j})} \otimes \vec{J}^{(\tilde{j}')} + \vec{J}^{(\tilde{j})} \otimes \mathbb{1}^{(\tilde{j}')} \right) | \psi_{\tilde{j}}, \psi_{\tilde{j}'} \rangle. \end{aligned} \quad (12)$$

This parametrization of $|\Psi_{\mathbf{J}}, \Psi_{\mathbf{J}^c}\rangle$ in terms of \vec{p} , \vec{p}' , $\{\psi_{\tilde{j}}\}_{\tilde{j} \in \mathcal{J}(\mathbf{J})}$, and $\{\psi_{\tilde{j}'}\}_{\tilde{j}' \in \mathcal{J}(\mathbf{J}^c)}$ simplifies Eq. (10) to

$$\begin{aligned} \max_{\rho_{\mathbf{J}, \mathbf{J}^c}} \text{tr} \left[\rho_{\mathbf{J}, \mathbf{J}^c} f(\vec{J}) \right] &= \max_{\vec{p}, \vec{p}'} \sum_{\tilde{j} \in \mathcal{J}(\mathbf{J}), \tilde{j}' \in \mathcal{J}(\mathbf{J}^c)} p_{\tilde{j}} p'_{\tilde{j}'} \left[\max_{|\psi_{\tilde{j}}, \psi_{\tilde{j}'}\rangle} \langle \psi_{\tilde{j}}, \psi_{\tilde{j}'} | f(\mathbb{1}^{(\tilde{j})} \otimes \vec{J}^{(\tilde{j}')} + \vec{J}^{(\tilde{j})} \otimes \mathbb{1}^{(\tilde{j}')}) | \psi_{\tilde{j}}, \psi_{\tilde{j}'} \rangle \right] \\ &= \max_{\tilde{j} \in \mathcal{J}(\mathbf{J}), \tilde{j}' \in \mathcal{J}(\mathbf{J}^c)} \left[\max_{|\psi_{\tilde{j}}, \psi_{\tilde{j}'}\rangle} \langle \psi_{\tilde{j}}, \psi_{\tilde{j}'} | f(\mathbb{1}^{(\tilde{j})} \otimes \vec{J}^{(\tilde{j}')} + \vec{J}^{(\tilde{j})} \otimes \mathbb{1}^{(\tilde{j}')}) | \psi_{\tilde{j}}, \psi_{\tilde{j}'} \rangle \right] \\ \therefore \max_{\rho_{\mathbf{J}, \mathbf{J}^c}} \text{tr} \left[\rho_{\mathbf{J}, \mathbf{J}^c} f \left(\sum_{j \in \mathbf{J} \cup \mathbf{J}^c} \vec{J}^{(j)} \right) \right] &= \max_{\tilde{j} \in \mathcal{J}(\mathbf{J}), \tilde{j}' \in \mathcal{J}(\mathbf{J}^c)} \left\{ \max_{\rho_{\{\tilde{j}\}, \{\tilde{j}'\}}} \text{tr} \left[\rho_{\{\tilde{j}\}, \{\tilde{j}'\}} f \left(\sum_{j \in \{\tilde{j}\} \cup \{\tilde{j}'\}} \vec{J}^{(j)} \right) \right] \right\}, \end{aligned} \quad (13)$$

where the second line follows from the maximization of the convex sum in the first, and the last line similarly follows from the convexity of separable states $\rho_{\{\tilde{j}\}, \{\tilde{j}'\}}$ in the subspace $\mathcal{H}^{(\tilde{j})} \otimes \mathcal{H}^{(\tilde{j}')}$.

Notably, each term in the braces in Eq. (13) is a maximization over separable states on the subspace of the tensor product of just the two fixed spins \tilde{j} and \tilde{j}' , and the observable is itself defined within that subspace. With $f(\vec{J}) = Q_K$ in Eq. (13) substituted into Eq. (7), the GME and bipartite separable bounds can be related as follows:

$$\mathbf{P}_K^{\text{sep}}(\{j_n\}_{n=1}^N) = \max_{\mathbf{J}} \max_{\substack{\tilde{j} \in \mathcal{J}(\mathbf{J}), \\ \tilde{j}' \in \mathcal{J}(\mathbf{J}^c)}} \mathbf{P}_K^{\text{sep}}(\{\tilde{j}, \tilde{j}'\}), \quad (14)$$

with $\mathbf{J} \in 2^{\{j_n\}_{n=1}^N} \setminus \{\emptyset, \{j_n\}_{n=1}^N\}$.

To evaluate $\mathbf{P}_K^{\text{sep}}(\{j_n\}_{n=1}^N)$, one first identifies the spins \tilde{j} and \tilde{j}' that appear in Eq. (14), evaluate $\mathbf{P}_K^{\text{sep}}(\{\tilde{j}, \tilde{j}'\})$ for each pair, and pick out the maximum value. This simplifies the process of calculating the multipartite separable bound, as it reduces it to the calculation of several bipartite separable bounds.

A possible hassle might come from iterating over the possible subsets \mathbf{J} , or from the tedium of working out the set of irreducible spins $\mathcal{J}(\mathbf{J})$. Closed-form expressions of \mathbf{J} and $\mathcal{J}(\mathbf{J})$ are known, and can be worked out algorithmically with a computer [48]. Alternatively, from the necessity that \tilde{j}, \tilde{j}' must be nonnegative, and that $\tilde{j} + \tilde{j}' \leq \sum_{n=1}^N j_n$ since they arise from the block decomposition of $\sum_{n=1}^N \vec{J}^{(j_n)}$, a convenient upper bound is

$$\mathbf{P}_K^{\text{sep}}(\{j_n\}_{n=1}^N) \leq \max_{\substack{0 \leq \tilde{j} + \tilde{j}' \leq \sum_{n=1}^N j_n, \\ \tilde{j}, \tilde{j}' \in \frac{1}{2}\mathbb{Z}_0^+}} \mathbf{P}_K^{\text{sep}}(\{\tilde{j}, \tilde{j}'\}), \quad (15)$$

where $\frac{1}{2}\mathbb{Z}_0^+$ is the set of positive integers and half-integers.

B. Trivial separable bounds for $\sum_{n=1}^N j_n < K/2$

For the special case $\sum_{n=1}^N j_n < K/2$, the separable bound can be calculated directly. By performing a sim-

ilar block decomposition to Eq. (8), the total angular momentum of the spin ensemble is

$$\vec{J} = \sum_{n=1}^N \vec{J}^{(j_n)} = \bigoplus_{j \in \mathcal{J}(\{j_n\}_{n=1}^N)} \vec{J}^{(j)}. \quad (16)$$

As before, the observable Q_K , which describes the precession protocol performed on the total angular momentum, will also inherit this block diagonal structure:

$$Q_K = \bigoplus_{j \in \mathcal{J}(\{j_n\}_{n=1}^N)} \frac{1}{K} \sum_{k=0}^{K-1} \text{pos}[J_k^{(j)}]. \quad (17)$$

$\underbrace{\hspace{10em}}_{=: Q_K^{(j)}}$

The eigendecomposition of $Q_K^{(j)}$ is known for some values of j [41]. In particular,

$$Q_K^{(j < K/2)} = \frac{1}{2} \mathbb{1}^{(j)}. \quad (18)$$

Since it must be that $j \leq \sum_{n=1}^N j_n$ for every $j \in \mathcal{J}(\{j_n\}_{n=1}^N)$,

$$Q_K = \bigoplus_{j \in \mathcal{J}(\{j_n\}_{n=1}^N)} \frac{1}{2} \mathbb{1}^{(j)} = \frac{1}{2} \mathbb{1}. \quad (19)$$

Hence, for a spin ensemble such that $\sum_{n=1}^N j_n < K/2$, $P_K = 1/2$ for every state of the system. This also trivially gives $\mathbf{P}_K^{\text{sep}}(\{j_n\}_{n=1}^N) = 1/2$, but since there are no states that can violate this separable bound, performing the precession protocol in this case does not reveal anything about the entanglement of the system.

C. Separable bounds for $\sum_{n=1}^N j_n = K/2$

For $\sum_{n=1}^N j_n = K/2$, the upper bound in Eq. (15) requires the values of $\mathbf{P}_K^{\text{sep}}(\{\tilde{j}, \tilde{j}'\})$ for every \tilde{j} and \tilde{j}' such that $\tilde{j} + \tilde{j}' \leq K/2$. Since the separable bounds for

$\tilde{j} + \tilde{j}' < K/2$ have already been evaluated in the previous section, we would only need to additionally work out $\mathbf{P}_K^{\text{sep}}(\{\tilde{j}, \tilde{j}'\})$ for $\tilde{j} + \tilde{j}' = K/2$.

Hence, it is adequate to first restrict ourselves to the $\mathcal{H}^{(\tilde{j})} \otimes \mathcal{H}^{(\tilde{j}')}$ subspace. A block decomposition similar to the one in Eq. (17) gives

$$Q_K = \bigoplus_{j=|\tilde{j}-\tilde{j}'|}^{\tilde{j}+\tilde{j}'=K/2} Q_K^{(j)} = \frac{1}{2} \left(\mathbb{1} - \mathbb{1}^{(j=K/2)} \right) \oplus Q_K^{(j=K/2)}, \quad (20)$$

where we used $Q_K^{(j < K/2)} = \mathbb{1}^{(j < K/2)}/2$. However, the eigendecomposition of $Q_K^{(j=K/2)}$ is [41]

$$Q_K^{(j=K/2)} = \frac{1}{2} \mathbb{1}^{(j=K/2)} + \frac{2^{-(K-1)}}{2} \binom{K-1}{\frac{K-1}{2}} \times \left(|\mathbf{P}_{+K}\rangle\langle\mathbf{P}_{+K}| - |\mathbf{P}_{-K}\rangle\langle\mathbf{P}_{-K}| \right), \quad (21)$$

where $|\mathbf{P}_{\pm K}\rangle = \left(\left| \frac{K}{2}, \frac{K}{2} \right\rangle \pm (-1)^{(K-1)/2} \left| \frac{K}{2}, -\frac{K}{2} \right\rangle \right) / \sqrt{2}$. Placing this back into Eq. (20),

$$Q_K = \frac{1}{2} \mathbb{1} + \frac{2^{-(K-1)}}{2} \binom{K-1}{\frac{K-1}{2}} \times \left(|\mathbf{P}_{+K}\rangle\langle\mathbf{P}_{+K}| - |\mathbf{P}_{-K}\rangle\langle\mathbf{P}_{-K}| \right). \quad (22)$$

Meanwhile, observing that the only way for $-\tilde{j} \leq \tilde{m} \leq \tilde{j}$ and $-\tilde{j}' \leq \tilde{m}' \leq \tilde{j}'$ to satisfy $\tilde{m} + \tilde{m}' = \pm K/2$ is to have $\tilde{m} = \pm \tilde{j}$ and $\tilde{m}' = \pm \tilde{j}'$, $|\mathbf{P}_{\pm K}\rangle$ is expressed in the $\{|\tilde{j}, \tilde{m}\rangle \otimes |\tilde{j}', \tilde{m}'\rangle\}_{\tilde{m}, \tilde{m}' = -\tilde{j}, -\tilde{j}'}$ basis as

$$|\mathbf{P}_{\pm K}\rangle = \frac{1}{\sqrt{2}} \left(|\tilde{j}, \tilde{j}\rangle \otimes |\tilde{j}', \tilde{j}'\rangle \pm (-1)^{(K-1)/2} |\tilde{j}, -\tilde{j}\rangle \otimes |\tilde{j}', -\tilde{j}'\rangle \right). \quad (23)$$

With this, we are now able to evaluate

$$\mathbf{P}_K^{\text{sep}}(\{\tilde{j}, \tilde{j}'\}) = \max_{|\psi_{\tilde{j}}, \psi_{\tilde{j}'}\rangle} \langle \psi_{\tilde{j}}, \psi_{\tilde{j}'} | Q_K | \psi_{\tilde{j}}, \psi_{\tilde{j}'} \rangle, \quad (24)$$

where $|\psi_{\tilde{j}}, \psi_{\tilde{j}'}\rangle = |\psi_{\tilde{j}}\rangle \otimes |\psi_{\tilde{j}'}\rangle$ with $|\psi_{\tilde{j}}\rangle \in \mathcal{H}^{(\tilde{j})}$ and $|\psi_{\tilde{j}'}\rangle \in \mathcal{H}^{(\tilde{j}')}$. Let us first parametrize the latter state as $|\psi_{\tilde{j}'}\rangle = \sum_{\tilde{m}' = -\tilde{j}'}^{\tilde{j}'} c_{\tilde{m}'} |\tilde{j}', \tilde{m}'\rangle$. Then,

$$\begin{aligned} & \left(\mathbb{1}^{(\tilde{j})} \otimes \langle \psi_{\tilde{j}'} | \right) Q_K \left(\mathbb{1}^{(\tilde{j})} \otimes |\psi_{\tilde{j}'}\rangle \right) \\ & \hat{=} \frac{1}{2} \mathbb{1}^{(\tilde{j})} + (-1)^{\frac{K-1}{2}} \frac{2^{-(K-1)}}{4} \binom{K-1}{\frac{K-1}{2}} \\ & \quad \times \begin{pmatrix} |c_{-\tilde{j}}|^2 & 0 & \dots & 0 & c_{-\tilde{j}}^* c_{+\tilde{j}} \\ 0 & 0 & \dots & 0 & 0 \\ \vdots & \ddots & & \vdots & \\ 0 & 0 & \dots & 0 & 0 \\ c_{-\tilde{j}} c_{+\tilde{j}}^* & 0 & \dots & 0 & |c_{+\tilde{j}}|^2 \end{pmatrix}, \end{aligned} \quad (25)$$

where the operator is represented as a matrix in the $\{|\tilde{j}, \tilde{m}\rangle\}_{\tilde{m} = -\tilde{j}}^{\tilde{j}}$ basis. Since $\max_{|\psi_{\tilde{j}}\rangle} \langle \psi_{\tilde{j}}, \psi_{\tilde{j}'} | Q_K | \psi_{\tilde{j}}, \psi_{\tilde{j}'} \rangle$ for

a fixed $|\psi_{\tilde{j}'}\rangle$ is the largest eigenvalue of the operator in Eq. (25), Eq. (24) can be evaluated by first diagonalizing Eq. (25) using standard analytical methods, then maximizing over $|\psi_{\tilde{j}'}\rangle$. Therefore,

$$\begin{aligned} \mathbf{P}_K^{K\text{-sep}} & := \mathbf{P}_K^{\text{sep}}(\{\tilde{j}, \tilde{j}'\}) \text{ for } \tilde{j} + \tilde{j}' = K/2 \\ & = \max_{|\psi_{\tilde{j}'}\rangle} \left(\max_{|\psi_{\tilde{j}}\rangle} \langle \psi_{\tilde{j}}, \psi_{\tilde{j}'} | Q_K | \psi_{\tilde{j}}, \psi_{\tilde{j}'} \rangle \right) \\ & = \max_{\{c_{\tilde{m}'}\}_{\tilde{m}'}} \left[\frac{1}{2} + \frac{2^{-(K-1)}}{4} \binom{K-1}{\frac{K-1}{2}} (|c_{-\tilde{j}'}|^2 + |c_{+\tilde{j}'}|^2) \right] \\ & = \frac{1}{2} \left[1 + 2^{-K} \binom{K-1}{\frac{K-1}{2}} \right]. \end{aligned} \quad (26)$$

Turning our attention back to the spin ensemble $\{j_n\}_{n=1}^N$ such that $\sum_{n=1}^N j_n = K/2$, Eq. (15) gives

$$\mathbf{P}_K^{\text{sep}}(\{j_n\}_{n=1}^N) \leq \max \left\{ 1/2, \mathbf{P}_K^{K\text{-sep}} \right\} = \mathbf{P}_K^{K\text{-sep}}, \quad (27)$$

where 1/2 appears in the maximization from the contribution of $\mathbf{P}_K^{\text{sep}}(\tilde{j}, \tilde{j}')$ for the case $\tilde{j} + \tilde{j}' < K/2$, while $\mathbf{P}_K^{K\text{-sep}}$ covers the $\tilde{j} + \tilde{j}' = K/2$ case.

From Eq. (27), Result 1 follows immediately.

Result 1. Consider an N -partite spin ensemble $\{j_n\}_{n=1}^N$ such that $\sum_{n=1}^N j_n = K/2$ for odd $K \geq 3$. Perform the precession protocol with K measurements on the total angular momentum of the system. If the score $P_K > \mathbf{P}_K^{K\text{-sep}}$ is obtained, where

$$\mathbf{P}_K^{K\text{-sep}} = \frac{1}{2} \left[1 + 2^{-K} \binom{K-1}{\frac{K-1}{2}} \right], \quad (28)$$

the spin ensemble is GME.

Note that $\mathbf{P}_K^{K\text{-sep}} < \mathbf{P}_K^c$ and $\mathbf{P}_K^{K\text{-sep}} > \mathbf{P}_K^c$. That is, violating the classical bound is sufficient for detecting entanglement when $\sum_{n=1}^N j_n \leq 5/2$, while a larger violation is required when $\sum_{n=1}^N j_n > 5/2$. Regardless, the violation only needs to be, at most, $\sim 3.9\%$ larger than the classical bound in the latter case: a loose upper bound is $\mathbf{P}_K^{K\text{-sep}} < 1.0391 \mathbf{P}_K^c$ for all K .

D. Separable bounds for general $\sum_{n=1}^N j_n$, fixed K

For spin ensembles with general $\sum_{n=1}^N j_n$, the values of $\mathbf{P}_K^{\text{sep}}(\{\tilde{j}, \tilde{j}'\})$ for $\tilde{j} + \tilde{j}' > K/2$ also come into play in Eq. (14). However, these bipartite separable bounds cannot be solved analytically, and we have to instead rely on numerical methods.

Two numerical methods were used to evaluate the bipartite separable bounds: the first is a variant of separability power iteration, which provides lower bounds [6]; the second is semidefinite programming, whose global convergence is guaranteed, which provides conservative

upper bounds [49]. Note that the latter is found by maximizing over a superset of the set of separable states that includes bound entangled states [50, 51], so the upper bounds might be loose in general.

Implementation of the numerical methods are detailed in Appendix D, while the scripts and generated data are available in Ref. [52]. By using both techniques, we are able to ascertain that the true value $\mathbf{P}_K^{\text{sep}*}$ falls within a range $\mathbf{P}_K^{\text{sep}} - \delta\mathbf{P}_K^{\text{sep}} \leq \mathbf{P}_K^{\text{sep}*} \leq \mathbf{P}_K^{\text{sep}} + \delta\mathbf{P}_K^{\text{sep}}$. The numerical errors $\delta\mathbf{P}_K^{\text{sep}}$ are plotted in Appendix A.

1. Numerical results for general $\{\tilde{j}, \tilde{j}'\}$, fixed K

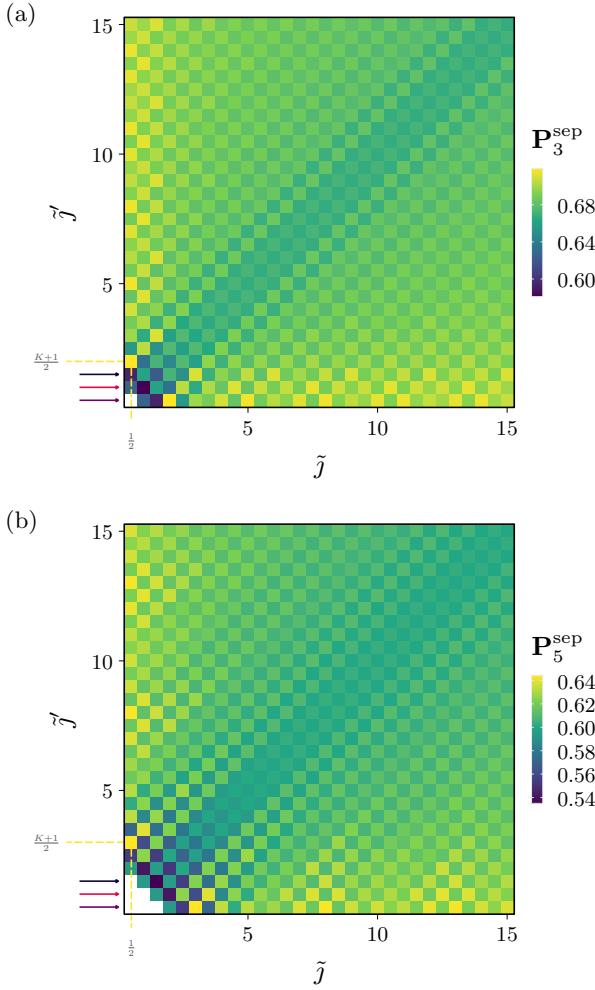


FIG. 2. Heatmap of $\mathbf{P}_K^{\text{sep}}(\{\tilde{j}, \tilde{j}'\})$ against \tilde{j} and \tilde{j}' , for (a) $K = 3$ and (b) $K = 5$. Note that the values $\mathbf{P}_K^{\text{sep}}(\{\tilde{j}, \tilde{j}'\}) = 1/2$ for $\tilde{j} + \tilde{j}' < K/2$ are neither plotted here nor for the subsequent figures. The separable bounds are large when $\min(\tilde{j}, \tilde{j}')$ is small, and $\mathbf{P}_K^{\text{sep}}$ decreases as $\min(\tilde{j}, \tilde{j}')$ increases. The maximum value of $\mathbf{P}_K^{\text{sep}}$ in these cases occur at $\{\tilde{j}, \tilde{j}'\} = \{1/2, (K+1)/2\}$. The colored arrows mark out the direction along which the line cuts in Fig. 4 are taken.

The plots of $\mathbf{P}_K^{\text{sep}}(\{\tilde{j}, \tilde{j}'\})$ against \tilde{j} and \tilde{j}' are shown in

Fig. 2 for $K = 3$ and $K = 5$. Notice that the separable bound is large for $\min(\tilde{j}, \tilde{j}') < 2$, and takes on smaller values as $\min(\tilde{j}, \tilde{j}')$ increases.

This behavior [that the separable bound is large when $\min(\tilde{j}, \tilde{j}')$ is small] can be found not just for $K = 7$ and $K = 9$, as plotted in Fig. 3, but up to $K = 21$, as plotted in Fig. A1. From the numerical results, we can find the values of $\{\tilde{j}, \tilde{j}'\}$ where the maximum occurs. As the gap between the largest and second largest value is larger than the numerical error, we can be certain that the largest computed value is indeed the maximum, leading us to the following result.

Result 2. *The maximum separable bound over $0 \leq \tilde{j}, \tilde{j}' \leq 15$ for fixed $3 \leq K \leq 21$ occurs at*

$$\operatorname{argmax}_{\{\tilde{j}, \tilde{j}'\}} \mathbf{P}_K^{\text{sep}}(\{\tilde{j}, \tilde{j}'\}) = \begin{cases} \{\frac{1}{2}, \frac{K+1}{2}\} & \text{for } K \leq 7, \\ \{1, \frac{K}{2}\} & \text{for } K \geq 7, \end{cases} \quad (29)$$

where $\operatorname{argmax}_x f(x) = \mathbf{x}$ such that $f(\mathbf{x}) = \max_x f(x)$.

Equation (29) is multivalued for $K = 7$ because, up to numerical precision, $\mathbf{P}_7^{\text{sep}}(\{1/2, 4\}) = \mathbf{P}_7^{\text{sep}}(\{1, 7/2\})$.

The numerical results for various values of K , especially when placed side-by-side as in Fig. A1, strongly suggest that these behaviors should hold for any value of K . As such, for a given K , it is worth identifying some trends about the values of $\{\tilde{j}, \tilde{j}'\}$ at which the maximum separable bound occurs.

For $K = 3, 5$, and 7 , the maximum values of $\mathbf{P}_K^{\text{sep}}$ that appear in Figs. 2 and 3(a) occur at $\{\tilde{j}, \tilde{j}'\} = \{1/2, (K+1)/2\}$. For a closer inspection, line cuts taken along $\tilde{j}' < 2$ are shown in Figs. 4 and 5. We find that for large \tilde{j} , the values of $\mathbf{P}_K^{\text{sep}}$ cluster around a range of values that are strictly smaller than the previously identified maximum score. As such, we can be reasonably sure that the maximum of $\mathbf{P}_K^{\text{sep}}$ over $0 \leq \tilde{j}, \tilde{j}' \leq \infty$ occurs at $\{\tilde{j}, \tilde{j}'\} = \{1/2, (K+1)/2\}$ for $K = 3, 5$, and 7 .

Meanwhile, for $7 \leq K \leq 21$, Figs. 3 and A1 clearly show that the maximums occur at $\{\tilde{j}, \tilde{j}'\} = \{1, K/2\}$, and the separable bound decreases sharply as \tilde{j} and \tilde{j}' increases. We conjecture that this pattern also holds for larger values of K , and in conjunction with the previous conjecture, we have the following.

Conjecture 1. *The maximum separable bound over $0 \leq \tilde{j}, \tilde{j}' \leq \infty$ for fixed K occurs at*

$$\operatorname{argmax}_{\{\tilde{j}, \tilde{j}'\}} \mathbf{P}_K^{\text{sep}}(\{\tilde{j}, \tilde{j}'\}) = \begin{cases} \{\frac{1}{2}, \frac{K+1}{2}\} & \text{for } K \leq 7, \\ \{1, \frac{K}{2}\} & \text{for } K \geq 7. \end{cases} \quad (30)$$

Having found the probable spins at which the maximum occurs, we shall now attempt to find the maximum separable bounds themselves. For $\{\tilde{j}, \tilde{j}'\} = \{1/2, (K+1)/2\}$, the separable bound can be exactly solved to be

$$\begin{aligned} & \mathbf{P}_K^{\text{sep}}\left(\left\{\frac{1}{2}, \frac{K+1}{2}\right\}\right) \\ &= \begin{cases} \frac{23}{32} & \text{if } K = 3, \text{ otherwise} \\ \frac{1}{2} \left[1 + \frac{2^{-(K+1)}}{K+1} \left(\frac{K-1}{\frac{K-1}{2}} \right) (K + \sqrt{3K^2 + 18K + 16}) \right]. \end{cases} \end{aligned} \quad (31)$$

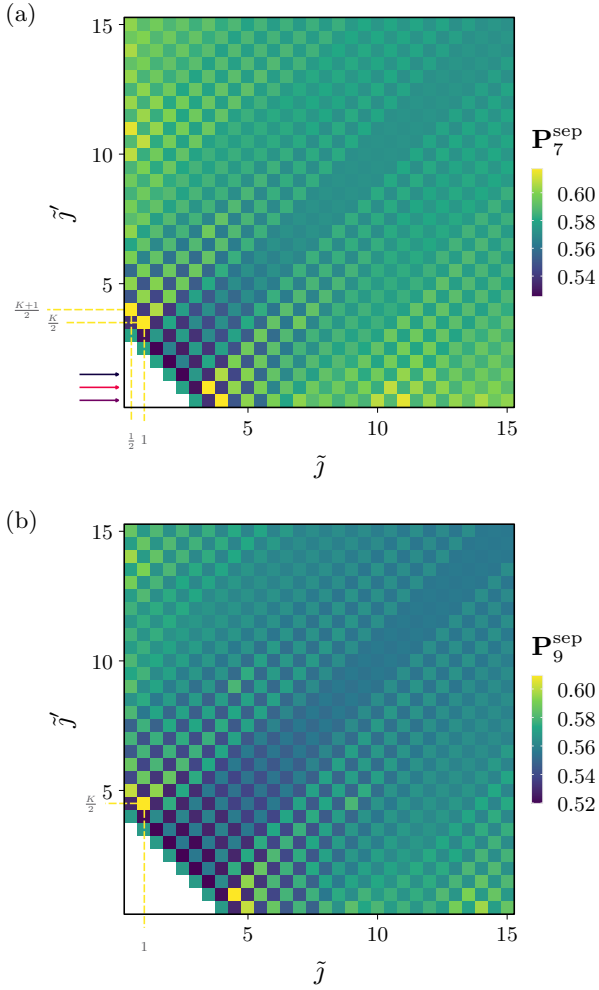


FIG. 3. Heatmap of $\mathbf{P}_K^{\text{sep}}(\{\tilde{j}, \tilde{j}'\})$ against \tilde{j} and \tilde{j}' , for (a) $K = 7$ and (b) $K = 9$. Similarly to Fig. 2, the separable bounds are large for small values of $\min(\tilde{j}, \tilde{j}')$. For $K = 7$, $\mathbf{P}_K^{\text{sep}}$ is maximal at both $\{\tilde{j}, \tilde{j}'\} = \{1/2, (K+1)/2\}$ and $\{1, K/2\}$. For $K = 9$, the maximum value occurs at $\{\tilde{j}, \tilde{j}'\} = \{1, K/2\}$. The colored arrows mark out the line cuts plotted in Fig. 5.

The derivation of Eq. (31) is given in Appendix C.

We were unable to apply the same analytical methods to $\{\tilde{j}, \tilde{j}'\} = \{1, K/2\}$, but we have a guess for the expression of the separable bound in that case.

Conjecture 2. *The separable bound for $\{\tilde{j}, \tilde{j}'\} = \{1, K/2\}$ with $K \geq 7$ is*

$$\mathbf{P}_K^{\text{sep}}(\{1, \frac{K}{2}\}) = \frac{1}{2} \left[1 + 2^{-(K-1)} \binom{K-1}{\frac{K-1}{2}} \frac{K-1}{K+1} \right]. \quad (32)$$

Note that $\mathbf{P}_K^{\text{sep}}(\{1, \frac{K}{2}\}) = 1/2$ for $K = 3$ and 5 , hence their exclusion from the conjecture. While we were unable to prove Eq. (32), it is in excellent agreement with the numerics up to $K = 101$, as shown in Fig. 6. Furthermore, Eqs. (31) and (32) are equal for $K = 7$, which is consistent with the two maximums in Fig. 5.

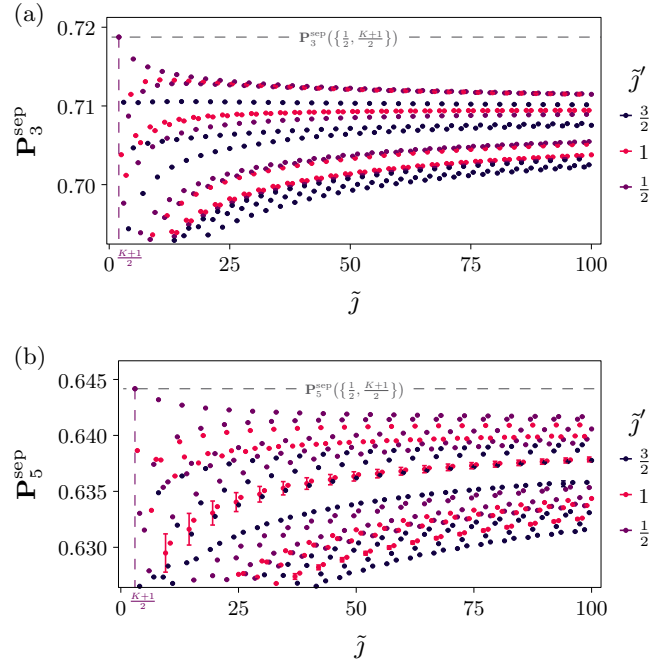


FIG. 4. Line cuts from Fig. 2 of (a) $\mathbf{P}_3^{\text{sep}}(\{\tilde{j}, \tilde{j}'\})$ and (b) $\mathbf{P}_5^{\text{sep}}(\{\tilde{j}, \tilde{j}'\})$ along fixed values of \tilde{j}' , plotted against a larger range of \tilde{j} . For this and subsequent line cuts, separable bounds for $\tilde{j} < \tilde{j}'$ are not shown; they can be obtained by swapping $\tilde{j} \leftrightarrow \tilde{j}'$. Note also that error bars $\pm \delta \mathbf{P}_K^{\text{sep}}(\{\tilde{j}, \tilde{j}'\})$ are drawn for every point, but most are too small to be visible. As \tilde{j} increases, $\mathbf{P}_K^{\text{sep}}$ clusters around a range of values that are strictly smaller than $\mathbf{P}_K^{\text{sep}}(\{1/2, (K+1)/2\})$. Due to this converging behavior for large \tilde{j} , we conjecture that the maximum value of $\mathbf{P}_K^{\text{sep}}(\{\tilde{j}, \tilde{j}'\})$ over $0 \leq \tilde{j}, \tilde{j}' \leq \infty$ occurs at $\{\tilde{j}, \tilde{j}'\} = \{1/2, (K+1)/2\}$ for $K = 3$ and $K = 5$.

Additionally, by taking the numerical precision into account, Eq. (32) can be turned into a reliable upper bound for Fig. 6.

Result 3. *The separable bound for $\{\tilde{j}, \tilde{j}'\} = \{1, K/2\}$ with $7 \leq K \leq 101$ is upper bounded by $\mathbf{P}_K^{\text{sep}}(\{1, \frac{K}{2}\}) + \delta \mathbf{P}_K^{\text{sep}}(\{1, \frac{K}{2}\})$, where $\delta \mathbf{P}_K^{\text{sep}} < 10^{-11}$ and*

$$\mathbf{P}_K^{\text{sep}}(\{1, \frac{K}{2}\}) = \frac{1}{2} \left[1 + 2^{-(K-1)} \binom{K-1}{\frac{K-1}{2}} \frac{K-1}{K+1} \right]. \quad (33)$$

We emphasize that Result 3, while numerical, is a definite result, as the global convergence of semi-definite programs guarantees that the computed values are reliable upper bounds.

2. Results and conjectures on separable bounds for general $\sum_{n=1}^N j_n$, fixed K

Finally, we can assemble the results and conjectures from the preceding sections to find a separable bound for a spin ensemble $\{j_n\}_{n=1}^N$ with general $\sum_{n=1}^N j_n$ and

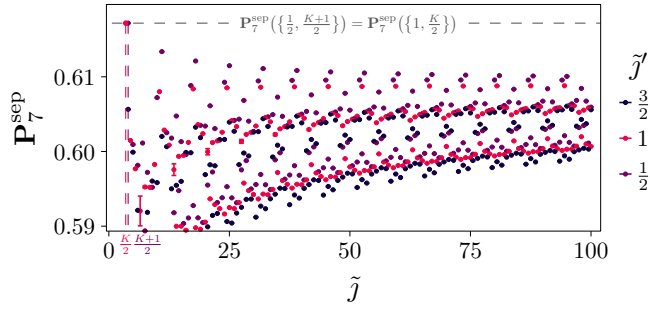


FIG. 5. Line cuts from Fig. 3(a) of $\mathbf{P}_7^{\text{sep}}(\{\tilde{j}, \tilde{j}'\})$ along fixed values of \tilde{j}' . Error bars $\pm \delta \mathbf{P}_7^{\text{sep}}(\{\tilde{j}, \tilde{j}'\})$ have been drawn for every point, but most are too small to be visible. Up to numerical precision, $\mathbf{P}_7^{\text{sep}}(\{1/2, 4\}) = \mathbf{P}_7^{\text{sep}}(\{1, 7/2\})$, and $\mathbf{P}_7^{\text{sep}}$ clusters around a range strictly smaller than $\mathbf{P}_7^{\text{sep}}(\{1/2, (K+1)/2\}) = \mathbf{P}_7^{\text{sep}}(\{1, K/2\})$. We conjecture that the $\mathbf{P}_7^{\text{sep}}(\{\tilde{j}, \tilde{j}'\})$ is maximal at both $\{\tilde{j}, \tilde{j}'\} = \{1/2, (K+1)/2\}$ and $\{1, K/2\}$.

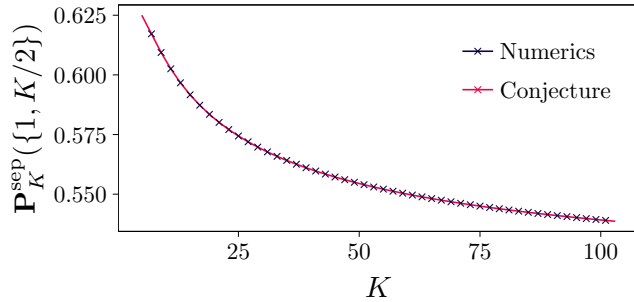


FIG. 6. The conjectured and numerically calculated separable bounds for $\{\tilde{j}, \tilde{j}'\} = \{1, K/2\}$. The numerical error $\delta \mathbf{P}_K^{\text{sep}} < 10^{-11}$ is too small to be plotted. This is in excellent agreement with Eq. (32) for all plotted values of $7 \leq K \leq 101$.

fixed K . Using the upper bounds on the bipartite separable bounds from Results 2 and 3, an upper bound on the multipartite separable bound can be found with Eq. (15).

Result 4. Consider an N -partite spin ensemble $\{j_n\}_{n=1}^N$ such that $\sum_{n=1}^N j_n \leq 15$. Perform the precession protocol with odd $3 \leq K \leq 21$ on the total angular momentum of the system. If the score $P_K > \mathbf{P}_K^{\text{conj}} + 10^{-11}$ is obtained, where

$$\mathbf{P}_K^{\text{conj}} := \begin{cases} \frac{23}{32} & \text{if } K = 3, \\ \frac{69 + \sqrt{181}}{128} & \text{if } K = 5, \\ \frac{1}{2} \left[1 + 2^{-(K-1)} \binom{K-1}{\frac{K-1}{2}} \frac{K-1}{K+1} \right] & \text{otherwise,} \end{cases}$$

the spin ensemble is GME.

Meanwhile, when the makeup of the spin ensemble is completely unknown, the only possible bound for the

total spin is $\sum_{n=1}^N j_n \leq \infty$, and the maximization in Eq. (15) would be over all possible $0 \leq \tilde{j}, \tilde{j}' \leq \infty$. While there are no analytical results in this case, Conjectures 1 and 2 can likewise be extended into a conjecture about the multipartite separable bound.

Conjecture 3. Consider a spin ensemble. Perform the precession protocol with odd $K \geq 3$ on the total angular momentum of the system. If the score $P_K > \mathbf{P}_K^{\text{conj}}$ is obtained, then the spin ensemble is GME.

IV. COMPARISON TO OTHER PROTOCOLS

A. Precession protocol as a quantum circuit

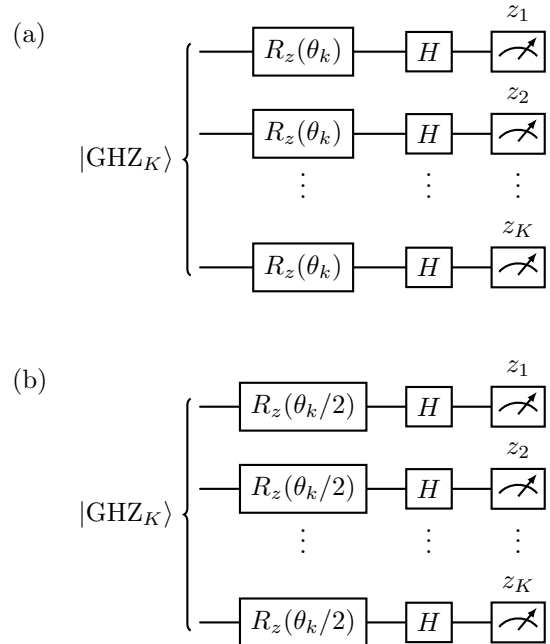


FIG. 7. The detection of GHZ entanglement as a quantum circuit, for (a) the precession protocol and (b) the fidelity-based witness. Here, $\theta_k = 2\pi k/K$, $R_z(\theta) = \exp(-i\theta\sigma_z/2)$ is a z -rotation gate, $H = (\sigma_x + \sigma_z)/\sqrt{2}$ is the Hadamard gate, and z_n is the outcome of σ_z on the n th qubit. For both witnesses, a measurement is performed for each θ_k with $k \in \{1, 2, \dots, K\}$, a collective quantity is calculated based on the outcomes $\{z_n\}_{n=1}^K$, and entanglement is detected when the average of this quantity over k violates some separable bound. Our PEW requires K measurement settings while the fidelity-based witness requires $K+1$ settings, and as such the former does not provide a significant improvement over the latter. Therefore, one might be better off using the fidelity-based witness in the context of quantum computation.

As the precession protocol can be performed with local spin measurements and classical post-processing, our PEW can also be implemented as a quantum circuit as

shown in Fig. 7(a). In this context, it is interesting to point out the similarities with the fidelity-based witness that is commonly used in the field of quantum computation [53], as is shown in Fig. 7(b).

(1) Both witnesses involve K equally distributed measurement settings: σ_{θ_k} for our PEW and $\sigma_{\theta_k/2}$ for the fidelity-based witness, where $\sigma_{\theta} = \cos\theta\sigma_x + \sin\theta\sigma_y$, $\sigma_s = J_s^{(j=1/2)}/2\hbar$ are the usual Pauli operators, and $\theta_k = 2\pi k/K$ for $k \in \{1, 2, \dots, K\}$.

(2) For each measurement setting k , a collective quantity is calculated from $\{z_n\}_{n=1}^K$, where z_n is the measurement outcome of σ_{θ} for the n th qubit. This is the majority $\Delta_k := \text{maj}(\{z_n\}_{n=1}^K)$ for our PEW, where $\text{maj}(\mathbf{S})$ returns the most commonly occurring value of the set \mathbf{S} , and the parity $\tilde{\Delta}_k := (-1)^k \prod_{n=1}^K z_n$ for the fidelity-based witness.

(3) Finally, entanglement is detected in both witnesses when the average of the collective quantity over all measurement settings violates some separable bound. This is $(1 + \frac{1}{K} \sum_{k=1}^K \Delta_k)/2 > \mathbf{P}_K^{K\text{-sep}}$ for our PEW, and $(1 - \frac{1}{K} \sum_{k=1}^K \tilde{\Delta}_k)/2 < \tilde{\Delta}_0/2$ for the fidelity-based witness, which requires an additional quantity $\tilde{\Delta}_0 := \langle (|\frac{K}{2}, \frac{K}{2}\rangle\langle\frac{K}{2}, \frac{K}{2}| + |\frac{K}{2}, -\frac{K}{2}\rangle\langle\frac{K}{2}, -\frac{K}{2}|) \rangle$ that can be computed by measuring all qubits in the σ_z basis.

As such, our PEW, which requires measuring in K different local bases, does not offer a significant improvement over the fidelity-based witness, which requires $K+1$ different local bases. Therefore, the fidelity-based witness might be a better choice if only individual addressing is available, as is usual in quantum computation.

B. Nondetection of highly symmetric states

A π rotation around the z axis, which acts as a parity operator for the eigenstates of J_z , has the action $e^{-i\pi J_z/\hbar} J_k e^{i\pi J_z/\hbar} = -J_k$ on the x - y plane, which implies $e^{-i\pi J_z/\hbar} Q_K e^{i\pi J_z/\hbar} = \mathbb{1} - Q_K$. Hence, for any state ρ such that $[e^{i\pi J_z/\hbar}, \rho] = 0$,

$$\text{tr}(\rho Q_K) = \text{tr}\left(e^{-i\pi J_z/\hbar} \rho e^{i\pi J_z/\hbar} Q_K\right) = 1 - \text{tr}(\rho Q_K). \quad (34)$$

As such, $\text{tr}(\rho Q_K) = 1/2 < \mathbf{P}_K^{K\text{-sep}} < \mathbf{P}_K^{\text{conj}}$ for any odd and finite K , so ρ does not violate the separable bound.

If $[e^{i\pi J_{\hat{n}}/\hbar}, \rho] \neq 0$ for another direction \hat{n} , the protocol can be performed with measurements in the plane perpendicular to \hat{n} , where there might possibly still be a violation of the separable bound.

However, if ρ commutes with the parity operator along every direction, then it will certainly not be detected by our witness. Hence, an important family of states that is missed by our protocol are the Werner states and their multipartite extensions [54, 55].

C. Nondetection of Dicke states

Another well-studied family of entangled states are the Dicke states

$$|D_l^n\rangle := \binom{n}{l}^{-\frac{1}{2}} \sum_{|\mathcal{P}|} \mathcal{P}\left(|\uparrow\rangle^{\otimes l} \otimes |\downarrow\rangle^{\otimes(n-l)}\right), \quad (35)$$

where the sum is over all permutations \mathcal{P} of the n spin-half states, with $|\uparrow\rangle := |\frac{1}{2}, \frac{1}{2}\rangle$ and $|\downarrow\rangle := |\frac{1}{2}, -\frac{1}{2}\rangle$. These include W states as members, and can be detected effectively using just spin angular momentum measurements [16, 18, 20, 22, 56–58]. Any of the referenced witnesses would be a better choice for detecting the entanglement of such states, as our witness is unable to detect the entanglement of Dicke states in general.

We note an exception: the tripartite Dicke or W state

$$|W_3\rangle := |D_1^3\rangle = \frac{1}{\sqrt{3}}(|\uparrow\downarrow\downarrow\rangle + |\downarrow\uparrow\downarrow\rangle + |\downarrow\downarrow\uparrow\rangle) \quad (36)$$

achieves $\langle W_3|Q_3|W_3\rangle = 11/16 > \mathbf{P}_3^{\text{conj}} > \mathbf{P}_3^{3\text{-sep}}$ when performing the precession protocol with measurements in the y - z plane. Hence, $|W_3\rangle$ is detected by our PEW, although this does not work beyond the tripartite case.

D. Detection of GHZ states

It follows directly from Eq. (22) that the precession protocol with K measurements can be used to detect the entanglement of the K -partite GHZ state, defined as

$$|\text{GHZ}_K\rangle := \frac{1}{\sqrt{2}}\left(|\uparrow\rangle^{\otimes K} + (-1)^{\frac{K-1}{2}} |\downarrow\rangle^{\otimes K}\right). \quad (37)$$

In fact, any GHZ state $\propto |\uparrow\rangle^{\otimes K} + e^{i\phi} |\downarrow\rangle^{\otimes K}$ with any phase $e^{i\phi}$ can be detected by the protocol with the replacement $J_k \rightarrow e^{-i\theta_i J_z/\hbar} J_k e^{i\theta_i J_z/\hbar}$, where $\theta_i = [(K-1)\pi - 2\phi]/(2K)$.

Meanwhile, a GHZ state in the presence of global depolarizing noise is given by

$$\rho_{\text{GHZ},K}^{(p_G)} := p_G \frac{\mathbb{1}}{\text{tr}(\mathbb{1})} + (1 - p_G) |\text{GHZ}_K\rangle\langle\text{GHZ}_K|, \quad (38)$$

which is GME if and only if $p_G < 1/[2(1 - 2^{-K})]$ [59]. This state achieves the score

$$\text{tr}\left(\rho_{\text{GHZ},K}^{(p_G)} Q_K\right) = \frac{1}{2} + 2(1 - p_G) \left(\mathbf{P}_K^{K\text{-sep}} - \frac{1}{2}\right). \quad (39)$$

If the total spin of the system is known to be $K/2$, our witness certifies GME when $\text{tr}(\rho_{\text{GHZ},K}^{(p_G)} Q_K) > \mathbf{P}_K^{K\text{-sep}}$, and hence is detected for the range $p_G < 1/2$. Therefore, our PEW can detect noisy GHZ states close to the theoretical limit.

As mentioned in the Introduction, GHZ states fail to be detected by almost every other angular-momentum-based witness mentioned in this paper [17, 19–22, 24,

35, 36]. The only exception is $|\text{GHZ}_3\rangle$, whose detection using angular momentum measurements is described in both Refs. [15] & [35]; but the reported methods do not work beyond the tripartite case.

E. Other states detected by our PEW

GHZ states are just one family of several that our PEW can detect, while possessing certain symmetries that prevent their detection by previous angular-momentum-based witness.

For a spin ensemble $\{j_n\}_{n=1}^N$ such that $\sum_{n=1}^N j_n$ is a half integer and $\sum_{n=1}^N j_n > K/2$, the $j = K/2$ subspace will be in general degenerate. Hence, the space of states that are eigenvalues of $Q_K^{(j=K/2)}$ with the same eigenvalue as $|\text{GHZ}_K\rangle$ will have a dimension larger than one, and any state that lives in this subspace will violate the separable bound and hence will be detected. A specific example for a spin-half ensemble with $N = 7$ particles that is detected by the precession protocol with $K = 5$ is

$$|\Phi_5\rangle := \frac{1}{2}\sqrt{\frac{7}{3}}\left(|\uparrow\rangle \otimes |\downarrow\rangle^{\otimes 6} - |\downarrow\rangle \otimes |\uparrow\rangle^{\otimes 6}\right) - \frac{1}{2\sqrt{3}}(|D_1^7\rangle - |D_6^7\rangle). \quad (40)$$

More generally, any state that lives in the subspace spanned by the eigenstates of Q_K whose eigenvalues are larger than the separable bound will be detected by our PEW. An example of this is

$$|\Phi_3\rangle := \frac{\sqrt{3}}{2}|\text{GHZ}_9\rangle - \frac{1}{2\sqrt{2}}(|D_3^9\rangle + |D_6^9\rangle), \quad (41)$$

which is also an eigenstate of Q_3 with an eigenvalue that is different from $\langle \text{GHZ}_3 | Q_3 | \text{GHZ}_3 \rangle$, but which nonetheless satisfies $\langle \Phi_3 | Q_3 | \Phi_3 \rangle > \mathbf{P}_3^{\text{conj}}$. Hence $|\Phi_3\rangle$, and indeed any superposition of $|\text{GHZ}_3\rangle$ and $|\Phi_3\rangle$, will be detected by the precession protocol with $K = 3$. We show in Appendix E that all of the discussed states ($|\text{GHZ}_K\rangle$, $|\Phi_5\rangle$, and $|\Phi_3\rangle$) are missed by all the other previously reported angular-momentum-based criteria, so these states can be detected only by our PEW.

The complete characterization of detectable states is still an open problem. This is partly because the eigen-decomposition of each block $Q_K^{(j)}$ is only known analytically for certain values of j , and partly because the space of detectable states depends on the degeneracy of each j , which, in turn, depends on the exact makeup of the ensemble. Regardless, with the above sufficient conditions, Q_K can be constructed numerically to find the subspace of states that will be detected by our PEW.

V. VARIATIONS ON THE PROTOCOL

A. Improved separable bound in the presence of more information

The reported results and conjectures heavily utilizes Eq. (14), which only takes into account the value of $\sum_{n=1}^N j_n$ and the score achieved when performing the precession protocol on the total angular momentum of the spin ensemble. No specific makeup of the spin ensemble $\{j_n\}_{n=1}^N$ was assumed.

Of course, more information can be obtained by characterizing the system in more detail or by performing other measurements. For example, if the system is a collection of bosons, the ensemble will be one of integer spins, and any fixed spin \tilde{j} that appears in the block decomposition of the total angular momentum must be a positive integer $\tilde{j} \in \mathbb{Z}_0^+$. Another example would be if the magnitude $|\tilde{J}|^2$ of the total angular momentum is measured in addition to performing the precession protocol, and was found take on possible values $j(j+1)$ for some $j \in \{j_{\min}, \dots, j_{\max}\}$. Then, the only spins \tilde{j} and \tilde{j}' that are compatible with the observed measurements of $|\tilde{J}|^2 = |\tilde{J}^{(\tilde{j})} + \tilde{J}^{(\tilde{j}')}|^2$ are those such that $|\tilde{j} - \tilde{j}'| \leq j_{\min}$ and $\tilde{j} + \tilde{j}' \geq j_{\max}$.

Just like the above two examples, any additional information about the system can restrict the possible spin pairs that appear in the maximization of Eq. (14). As this results in a maximization over a restricted range of arguments, the separable bound can be possibly lowered, requiring less violation to detect entanglement.

B. Constructing other witnesses using Sec. III A

A relation between the multipartite and bipartite separable bounds derived in Sec. III A was used in the process of constructing our PEW. This relation can be used to construct other entanglement witnesses. For example, consider performing the precession protocol with K measurements on a spin ensemble with total spin $K/2$ for K odd, but with the replacement $\text{pos}(J_k) \rightarrow f_0 \mathbb{1} + f_{\text{odd}}(J_k)$ with some odd function $f_{\text{odd}}(-x) = -f_{\text{odd}}(x)$. A similar analysis to Sec. III C gives the separable bound

$$\begin{aligned} \min_{\rho_{\text{sep}}} \text{tr} \left\{ \rho_{\text{sep}} \frac{1}{K} \sum_{k=0}^{K-1} [f_0 \mathbb{1} + f_{\text{odd}}(J_k)] \right\} \\ = f_0 + \frac{1}{2} \left| \langle \frac{K}{2}, \frac{K}{2} | f_{\text{odd}}(J_x) | \frac{K}{2}, -\frac{K}{2} \rangle \right| \end{aligned} \quad (42)$$

when minimized over separable states ρ_{sep} . This means that GHZ states will be detected by this modified witness as long as $f_K > 0$, which requires $\frac{d^{K+2L}}{dx^{K+2L}} f_{\text{odd}}(x)|_{x=0} \neq 0$ for some integer $L \geq 0$. Of course, by choosing $f_{\text{odd}}(x) \propto 2 \text{pos}(x) - 1$ as we do here, the magnitudes of the angular momentum measurements do not need to be resolved,

which is a benefit that might be lost with other choices of $f_{\text{odd}}(x)$.

On closer inspection, the relation derived in Sec. III A is not specific to our PEW, and is in fact applicable to any function $f(\vec{J})$ of angular momentum.

To illustrate this, consider the commonly used witness $|\vec{J}|^2$: given $g^{\text{sep}} := \min_{\rho_{\text{sep}}} \text{tr}(\rho_{\text{sep}} |\vec{J}|^2)$ minimized over separable states ρ_{sep} , $\langle |\vec{J}|^2 \rangle < g^{\text{sep}}$ implies entanglement [17, 24]. This witness corresponds to setting $f(\vec{J}) = -|\vec{J}|^2$ in Eq. (13), and the bipartite separable bound can be worked out to be

$$\begin{aligned}
g^{\text{sep}}(\{j_1, j_2\}) &= \min_{|\psi_{j_1}, \psi_{j_2}\rangle} \langle \psi_{j_1}, \psi_{j_2} | \left| \vec{J}^{(j_1)} + \vec{J}^{(j_2)} \right|^2 | \psi_{j_1}, \psi_{j_2} \rangle \\
&= \min_{|\psi_{j_1}, \psi_{j_2}\rangle} \left(\overbrace{\langle \psi_{j_1} | \left| \vec{J}^{(j_1)} \right|^2 | \psi_{j_1} \rangle}^{\hbar^2(j_1^2 + j_1)} + \overbrace{\langle \psi_{j_2} | \left| \vec{J}^{(j_2)} \right|^2 | \psi_{j_2} \rangle}^{\hbar^2(j_2^2 + j_2)} \right. \\
&\quad \left. + 2 \underbrace{\langle \psi_{j_1} | \vec{J}^{(j_1)} | \psi_{j_1} \rangle \cdot \langle \psi_{j_2} | \vec{J}^{(j_2)} | \psi_{j_2} \rangle}_{\geq -\sqrt{|\langle \psi_{j_1} | \vec{J}^{(j_1)} | \psi_{j_1} \rangle|^2 |\langle \psi_{j_2} | \vec{J}^{(j_2)} | \psi_{j_2} \rangle|^2}} \right) \\
&\quad \geq \hbar^2[(j_1 - j_2)^2 + (j_1 + j_2)], \tag{43}
\end{aligned}$$

with equality $g^{\text{sep}}(\{j_1, j_2\}) = \hbar^2[(j_1 - j_2)^2 + (j_1 + j_2)]$ as setting $|\psi_{j_n}\rangle = |j_n, (-1)^n j_n\rangle$ saturates Eq. (43). Substituting this into Eq. (13) gives $g^{\text{sep}}(\{j_n\}_{n=1}^N) = \hbar^2 \min_{\tilde{j}, \tilde{j}'} [(\tilde{j} - \tilde{j}')^2 + (\tilde{j} + \tilde{j}')]$ for all bipartitions \mathbf{J}, \mathbf{J}^c , $\tilde{j} \in \mathcal{J}(\mathbf{J})$, and $\tilde{j}' \in \mathcal{J}(\mathbf{J}^c)$.

As long as the singlet subspace of the chosen spin ensemble is nondegenerate, at least one of \tilde{j} or \tilde{j}' will be larger than zero, so $g^{\text{sep}}(\{j_n\}_{n=1}^N) > 0$. Meanwhile, if the singlet subspace exists, the corresponding singlet state achieves $\langle |\vec{J}|^2 \rangle = 0 < g^{\text{sep}}(\{j_n\}_{n=1}^N)$, and hence will be detected to be GME. This method is particularly useful for witnessing GME of unequal spins with the observable $|\vec{J}|^2$, which, to the best of our knowledge, has yet to be explored. As an example, take $\{j_n\}_{n=1}^4 = \{\frac{1}{2}, \frac{1}{2}, 1, 2\}$. Minimizing over all possible pairs $\{\tilde{j}, \tilde{j}'\}$ that arise, we find that $g^{\text{sep}}(\{j_n\}_n) = 1$. At the same time, the chosen spins permit a singlet subspace for $j = |(j_1 + j_2 + j_3) - j_4| = |\frac{1}{2} + \frac{1}{2} + 1 - 2| = 0$, so the GME of the corresponding singlet state can be detected.

More generally, Eq. (13) can be used to construct other GME witnesses by choosing other functions of $f(\vec{J})$. As demonstrated here, this approach allows us to extend existing bipartite witnesses into GME witnesses, which is especially convenient if an analytical form of the bipartite separable bound is known.

C. Bipartite separable bounds When $\tilde{j} = \tilde{j}'$ for fixed K

An interesting observation can be made about the behavior of the separable bound along the $\tilde{j} = \tilde{j}'$ diagonal. In Figs. 2, 3, and A1, the separable bounds along these diagonals are smaller in magnitude than the surrounding values, and seem to stabilize to a limit for large \tilde{j} .

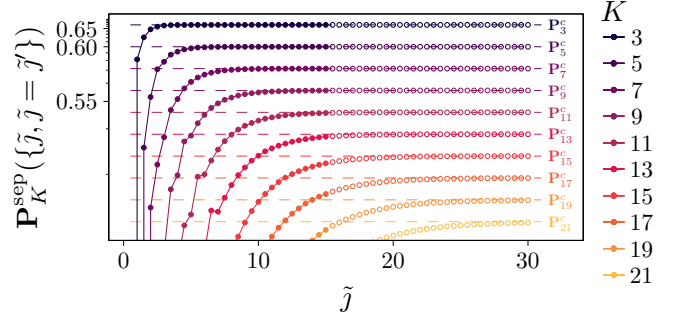


FIG. 8. Line cuts along the diagonals $\tilde{j} = \tilde{j}'$ along Figs. 2, 3, and A1. The vertical axis is scaled to fit every case, and the dashed lines are the classical bounds \mathbf{P}_K^c . The unfilled points mark those where only the lower bound $\mathbf{P}_K^{\text{sep}} - \delta \mathbf{P}_K^{\text{sep}}$ could be computed. For the filled points, the error bars $\delta \mathbf{P}_K^{\text{sep}}$ are smaller than the marker size. We find that $\mathbf{P}_K^{\text{sep}}(\{\tilde{j}, \tilde{j}'\})$ approaches \mathbf{P}_K^c from below as \tilde{j} increases.

Indeed, isolating these diagonals in Fig. 8 reveals that $\mathbf{P}_K^{\text{sep}}(\{\tilde{j}, \tilde{j}' = \tilde{j}\})$ approaches the classical bound \mathbf{P}_K^c from below as \tilde{j} increases.

This behavior is in accordance with two previously known results. First, the observable $\text{pos}(J_x^{(j)})$ has the limit $\lim_{j \rightarrow \infty} \text{pos}(J_x^{(j)}) = \text{pos}(a + a^\dagger)$ for the annihilation operator a of a harmonic oscillator. Second, for two harmonic oscillators with annihilation operators a_1 and a_2 , respectively, if the precession protocol is performed on the normal mode $a_+ \propto a_1 + a_2$, \mathbf{P}_K^c is the maximum score achievable by a state separable over the $\{a_1, a_2\}$ modes.

Therefore, as $J_x = J_x^{(\tilde{j})} + J_x^{(\tilde{j}')}$ for $\tilde{j} = \tilde{j}'$ appears analogous to $a_+ \propto a_1 + a_2$, it would be expected that $\lim_{\tilde{j} \rightarrow \infty} \text{pos}(J_x) \stackrel{?}{=} \text{pos}(a_+ + a_+^\dagger)$. If so, the separable bound should similarly have the limit $\lim_{\tilde{j} \rightarrow \infty} \mathbf{P}_K^{\text{sep}}(\{\tilde{j}, \tilde{j}' = \tilde{j}\}) \stackrel{?}{=} \mathbf{P}_K^c$. We have not managed to prove this, but Fig. 8 certainly supports this expectation, and suggests the following.

Conjecture 4. Consider a bipartite spin ensemble $\{\tilde{j}, \tilde{j}'\}$, where $\tilde{j} = \tilde{j}'$. Perform the precession protocol with odd $K \geq 3$ on the total angular momentum of the system. If the classical bound \mathbf{P}_K^c is violated, then the two spins are entangled.

While this conjecture is limited to the bipartite witness, it hints at a possible link between the classical bound of

the precession protocol, entanglement, and the harmonic oscillator limit.

VI. CONCLUSION

In this work, we introduced entanglement witnesses that detect genuine multipartite entanglement of a spin ensemble, which require only measurements of the total angular momentum along several equally spaced directions. We reported analytical expressions for the separable bound when the total spin is a half-integer. For the other cases, reliable numerical values and a conjectured expression is reported for the separable bound, where the latter is well supported by the former.

Of similar angular-momentum-based witnesses, only some detect genuine multipartite entanglement; of those that do, most are effective at detecting Dicke-like states, but none can detect Greenberger-Horne-Zeilinger states beyond the tripartite case. This gap is filled by our PEW, which is effective at detecting precisely those states. We also showed that our witness can detect other GME states, which share similar symmetries to the GHZ state, that are missed by existing criteria.

A possible extension would be to consider the effects of anharmonicities when performing the precession protocol under the assumption of dynamics. A popular experimental platform where spin ensembles naturally arise are spin defects or donors in solid-state materials [10, 11], where quadrupole interactions are present in the Hamiltonian as terms quadratic in angular momentum, which

perturbs the dynamics of the system away from a perfectly uniform precession. Such anharmonic effects have been studied for continuous variable systems [42], and many of those findings could be extended to the case of spin angular momentum.

Finally, we once again highlight the generality of the result in Sec. III A. By choosing different functions of angular momentum to be used with Eq. (13), it provides a generic recipe for constructing witnesses of genuine multipartite entanglement out of witnesses of bipartite entanglement. This can be applicable to many other entanglement witnesses completely unrelated to the precession protocol, as we showed with an example in the previous section. This provides another avenue for future study: Since our PEW is mostly effective when the total spin is a half-integer, and cannot witness inseparable states with positive partial transpose, these techniques might allow us to construct a similar witness that will also be effective for integral total spin or bound entangled states.

ACKNOWLEDGMENTS

Hung Nguyen Quoc is thanked by K.N.H.V. for his mentorship, and by V.S. for his hospitality at VNU, Hanoi.

This work is supported by the National Research Foundation, Singapore, and A*STAR under its CQT Bridging Grant. We also thank the National University of Singapore Information Technology for the use of their high performance computing resources.

-
- [1] O. Gühne and G. Tóth, Entanglement detection, *Physics Reports* **474**, 1 (2009).
 - [2] G. Tóth and I. Apellaniz, Quantum metrology from a quantum information science perspective, *Journal of Physics A: Mathematical and Theoretical* **47**, 424006 (2014).
 - [3] N. Friis, G. Vitagliano, M. Malik, and M. Huber, Entanglement certification from theory to experiment, *Nature Reviews Physics* **1**, 72 (2019).
 - [4] R. Horodecki, P. Horodecki, M. Horodecki, and K. Horodecki, Quantum entanglement, *Rev. Mod. Phys.* **81**, 865 (2009).
 - [5] J. Sperling and W. Vogel, Multipartite Entanglement Witnesses, *Phys. Rev. Lett.* **111**, 110503 (2013).
 - [6] S. Gerke, W. Vogel, and J. Sperling, Numerical construction of multipartite entanglement witnesses, *Phys. Rev. X* **8**, 031047 (2018).
 - [7] C. Branciard, D. Rosset, Y.-C. Liang, and N. Gisin, Measurement-Device-Independent Entanglement Witnesses for All Entangled Quantum States, *Phys. Rev. Lett.* **110**, 060405 (2013).
 - [8] M. C. Tran, B. Dakić, F. Arnault, W. Laskowski, and T. Paterek, Quantum entanglement from random measurements, *Phys. Rev. A* **92**, 050301(R) (2015).
 - [9] F. Schäfer, T. Fukuhara, S. Sugawa, Y. Takasu, and Y. Takahashi, Tools for quantum simulation with ultracold atoms in optical lattices, *Nature Reviews Physics* **2**, 411 (2020).
 - [10] G. Wolfowicz, F. J. Heremans, C. P. Anderson, S. Kanai, H. Seo, A. Gali, G. Galli, and D. D. Awschalom, Quantum guidelines for solid-state spin defects, *Nature Reviews Materials* **6**, 906 (2021).
 - [11] I. Fernández de Fuentes, T. Botzem, M. A. I. Johnson, A. Vaartjes, S. Asaad, V. Mourik, F. E. Hudson, K. M. Itoh, B. C. Johnson, A. M. Jakob, J. C. McCallum, D. N. Jamieson, A. S. Dzurak, and A. Morello, Navigating the 16-dimensional hilbert space of a high-spin donor qubit with electric and magnetic fields, *Nature Communications* **15**, 1380 (2024).
 - [12] A. S. Sørensen and K. Mølmer, Entanglement and Extreme Spin Squeezing, *Phys. Rev. Lett.* **86**, 4431 (2001).
 - [13] L. Pezzè, A. Smerzi, M. K. Oberthaler, R. Schmied, and P. Treutlein, Quantum metrology with nonclassical states of atomic ensembles, *Rev. Mod. Phys.* **90**, 035005 (2018).
 - [14] A. Sørensen, L.-M. Duan, J. I. Cirac, and P. Zoller, Many-particle entanglement with bose-einstein condensates, *Nature* **409**, 63 (2001).
 - [15] J. K. Korbicz, J. I. Cirac, and M. Lewenstein, Spin Squeezing Inequalities and Entanglement of N Qubit States, *Phys. Rev. Lett.* **95**, 120502 (2005).

- [16] J. K. Korbicz, O. Gühne, M. Lewenstein, H. Häffner, C. F. Roos, and R. Blatt, Generalized spin-squeezing inequalities in n -qubit systems: Theory and experiment, *Phys. Rev. A* **74**, 052319 (2006).
- [17] G. Tóth, Entanglement detection in optical lattices of bosonic atoms with collective measurements, *Phys. Rev. A* **69**, 052327 (2004).
- [18] G. Tóth, Detection of multipartite entanglement in the vicinity of symmetric Dicke states, *J. Opt. Soc. Am. B* **24**, 275 (2007).
- [19] G. Tóth, C. Knapp, O. Gühne, and H. J. Briegel, Optimal Spin Squeezing Inequalities Detect Bound Entanglement in Spin Models, *Phys. Rev. Lett.* **99**, 250405 (2007).
- [20] G. Tóth, C. Knapp, O. Gühne, and H. J. Briegel, Spin squeezing and entanglement, *Phys. Rev. A* **79**, 042334 (2009).
- [21] G. Vitagliano, P. Hyllus, I. L. Egusquiza, and G. Tóth, Spin Squeezing Inequalities for Arbitrary Spin, *Phys. Rev. Lett.* **107**, 240502 (2011).
- [22] G. Vitagliano, I. Apellaniz, I. L. Egusquiza, and G. Tóth, Spin squeezing and entanglement for an arbitrary spin, *Phys. Rev. A* **89**, 032307 (2014).
- [23] M. R. Dowling, A. C. Doherty, and S. D. Bartlett, Energy as an entanglement witness for quantum many-body systems, *Phys. Rev. A* **70**, 062113 (2004).
- [24] G. Tóth, Entanglement witnesses in spin models, *Phys. Rev. A* **71**, 010301(R) (2005).
- [25] S. M. Giampaolo and B. C. Hiesmayr, Genuine multipartite entanglement in the XY model, *Phys. Rev. A* **88**, 052305 (2013).
- [26] F. Iglói and G. Tóth, Entanglement witnesses in the XY chain: Thermal equilibrium and postquench nonequilibrium states, *Phys. Rev. Res.* **5**, 013158 (2023).
- [27] T. Homayoun and K. Aghayar, Energy as an entanglement witnesses for one dimensional XYZ Heisenberg lattice: Optimization approach, *Journal of Statistical Physics* **176**, 85 (2019).
- [28] L.-A. Wu, S. Bandyopadhyay, M. S. Sarandy, and D. A. Lidar, Entanglement observables and witnesses for interacting quantum spin systems, *Phys. Rev. A* **72**, 032309 (2005).
- [29] F. Troiani and I. Siloi, Energy as a witness of multipartite entanglement in chains of arbitrary spins, *Phys. Rev. A* **86**, 032330 (2012).
- [30] A. Gabriel and B. C. Hiesmayr, Macroscopic observables detecting genuine multipartite entanglement and partial inseparability in many-body systems, *Europhysics Letters* **101**, 30003 (2013).
- [31] J. Uffink, Quadratic Bell Inequalities as Tests for Multipartite Entanglement, *Phys. Rev. Lett.* **88**, 230406 (2002).
- [32] W. Dür, G. Vidal, and J. I. Cirac, Three qubits can be entangled in two inequivalent ways, *Phys. Rev. A* **62**, 062314 (2000).
- [33] O. Gühne, G. Tóth, and H. J. Briegel, Multipartite entanglement in spin chains, *New Journal of Physics* **7**, 229 (2005).
- [34] O. Gühne and G. Tóth, Energy and multipartite entanglement in multidimensional and frustrated spin models, *Phys. Rev. A* **73**, 052319 (2006).
- [35] R. Y. Teh and M. D. Reid, Criteria to detect genuine multipartite entanglement using spin measurements, *Phys. Rev. A* **100**, 022126 (2019).
- [36] J. Li and L. Chen, Detection of genuine multipartite entanglement based on uncertainty relations, *Quantum Information Processing* **20**, 220 (2021).
- [37] R. H. Dicke, Coherence in spontaneous radiation processes, *Phys. Rev.* **93**, 99 (1954).
- [38] E. D'Hondt and P. Panangaden, The computational power of the W and GHZ states, *Quantum Inf. Comput.* **6**, 173 (2006).
- [39] A. Broadbent, P.-R. Chouha, and A. Tapp, The GHZ State in Secret Sharing and Entanglement Simulation, in *2009 Third International Conference on Quantum, Nano and Micro Technologies* (IEEE, New York, 2009) pp. 59–62.
- [40] B. Tsirelson, How often is the coordinate of a harmonic oscillator positive? (2006), [arXiv:quant-ph/0611147 \[quant-ph\]](https://arxiv.org/abs/quant-ph/0611147).
- [41] L. H. Zaw, C. C. Aw, Z. Lasmar, and V. Scarani, Detecting quantumness in uniform precessions, *Phys. Rev. A* **106**, 032222 (2022).
- [42] L. H. Zaw and V. Scarani, Dynamics-based quantumness certification of continuous variables using time-independent hamiltonians with one degree of freedom, *Phys. Rev. A* **108**, 022211 (2023).
- [43] P. Jayachandran, L. H. Zaw, and V. Scarani, Dynamics-Based Entanglement Witnesses for Non-Gaussian States of Harmonic Oscillators, *Phys. Rev. Lett.* **130**, 160201 (2023).
- [44] R. Ghosh and S. Bose, Separability criterion using one observable for special states: Entanglement detection via quantum quench (2023), [arXiv:2307.03735 \[quant-ph\]](https://arxiv.org/abs/2307.03735).
- [45] F. Schäfer, M. Kloc, C. Bruder, and N. Lörch, A differentiable programming method for quantum control, *Machine Learning: Science and Technology* **1**, 035009 (2020).
- [46] E. Takou, E. Barnes, and S. E. Economou, Generation of genuine all-way entanglement in defect-nuclear spin systems through dynamical decoupling sequences (2023), [arXiv:2302.05580 \[quant-ph\]](https://arxiv.org/abs/2302.05580).
- [47] A. Edmonds, *Angular Momentum in Quantum Mechanics*, Investigations in Physics (Princeton University Press, Princeton, NJ, 1960).
- [48] V. V. Mikhailov, Addition of an arbitrary number of different angular momenta, *J. Phys. A* **14**, 1107 (1981).
- [49] L. Vandenberghe and S. Boyd, Semidefinite programming, *SIAM Review* **38**, 49 (1996).
- [50] M. Horodecki, P. Horodecki, and R. Horodecki, Mixed-State Entanglement and Distillation: Is there a “Bound” Entanglement in Nature?, *Phys. Rev. Lett.* **80**, 5239 (1998).
- [51] G. Tóth and O. Gühne, Entanglement and Permutational Symmetry, *Phys. Rev. Lett.* **102**, 170503 (2009).
- [52] L. H. Zaw, Script used in: Certification of genuine multipartite entanglement in spin ensembles with measurements of total angular momentum [[arXiv:2210.10357](https://arxiv.org/abs/2210.10357)], <https://github.com/not-fred/arXiv-2311.00806> (2023).
- [53] O. Gühne, C.-Y. Lu, W.-B. Gao, and J.-W. Pan, Toolbox for entanglement detection and fidelity estimation, *Phys. Rev. A* **76**, 030305(R) (2007).
- [54] R. F. Werner, Quantum states with einstein-podolsky-rosen correlations admitting a hidden-variable model, *Phys. Rev. A* **40**, 4277 (1989).
- [55] T. Eggeling, *On multipartite symmetric states in Quantum Information Theory*, Ph.D. thesis, Technische Universität Braunschweig (2003).

- [56] M. Huber, P. Erker, H. Schimpf, A. Gabriel, and B. Hiesmayr, Experimentally feasible set of criteria detecting genuine multipartite entanglement in n -qubit dicke states and in higher-dimensional systems, *Phys. Rev. A* **83**, 040301(R) (2011).
- [57] L.-M. Duan, Entanglement Detection in the Vicinity of Arbitrary Dicke States, *Phys. Rev. Lett.* **107**, 180502 (2011).
- [58] B. Lücke, J. Peise, G. Vitagliano, J. Arlt, L. Santos, G. Tóth, and C. Klempt, Detecting Multiparticle Entanglement of Dicke States, *Phys. Rev. Lett.* **112**, 155304 (2014).
- [59] O. Gühne and M. Seevinck, Separability criteria for genuine multiparticle entanglement, *New Journal of Physics* **12**, 053002 (2010).
- [60] A. Peres, Separability Criterion for Density Matrices, *Phys. Rev. Lett.* **77**, 1413 (1996).
- [61] M. Horodecki, P. Horodecki, and R. Horodecki, Separability of mixed states: necessary and sufficient conditions, *Physics Letters A* **223**, 1 (1996).
- [62] M. Lubin, O. Dowson, J. Dias Garcia, J. Huchette, B. Legat, and J. P. Vielma, JuMP 1.0: Recent improvements to a modeling language for mathematical optimization, *Mathematical Programming Computation* [10.1007/s12532-023-00239-3](https://doi.org/10.1007/s12532-023-00239-3) (2023).
- [63] M. Garstka, M. Cannon, and P. Goulart, COSMO: A conic operator splitting method for convex conic problems, *Journal of Optimization Theory and Applications* **190**, 779 (2021).
- [64] P. van Loock and A. Furusawa, Detecting genuine multipartite continuous-variable entanglement, *Phys. Rev. A* **67**, 052315 (2003).

Appendix A: Additional Figures

Some additional figures are gathered in this appendix. Figure A1 plots $\mathbf{P}_K^{\text{sep}}$ for $11 \leq K \leq 21$, which complements Figs. 2 and 3; Fig. A2 plots the discrepancy $\delta\mathbf{P}_K^{\text{sep}}$ between the numerically computed lower and upper bounds of $\mathbf{P}_K^{\text{sep}}$, as detailed in Appendix. D; Fig. A3 plots the lower bound of $\mathbf{P}_K^{\text{sep}}$ for a wider range of \tilde{j} and \tilde{j}' , demonstrating that the expected behavior of $\mathbf{P}_K^{\text{sep}}$ appears to hold for larger values of \tilde{j} and \tilde{j}' , providing further support for Conjecture 3.

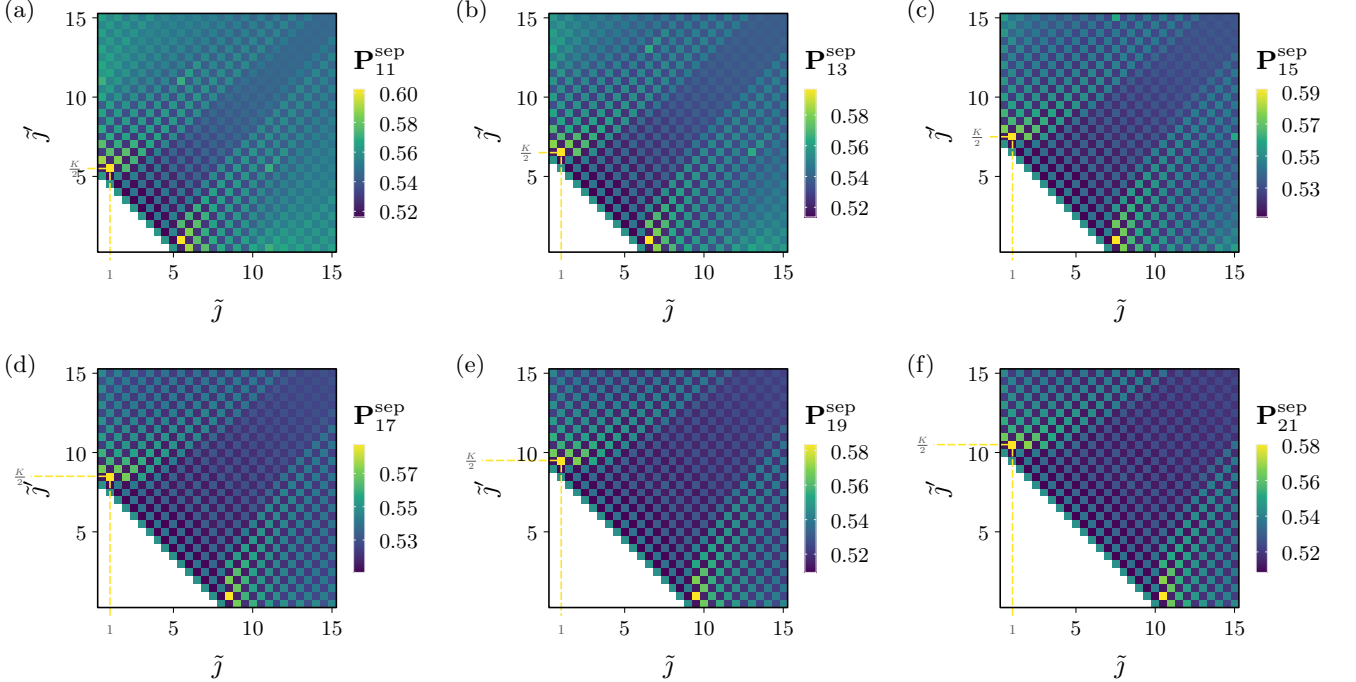


FIG. A1. Heatmap of $\mathbf{P}_K^{\text{sep}}(\{\tilde{j}, \tilde{j}'\})$ against \tilde{j} and \tilde{j}' , for (a) $K = 11$, (b) $K = 13$, (c) $K = 15$, (d) $K = 17$, (e) $K = 19$, and (f) $K = 21$. The values $\mathbf{P}_K^{\text{sep}}(\{\tilde{j}, \tilde{j}'\}) = 1/2$ for $\tilde{j} + \tilde{j}' < K/2$ are not plotted here. The separable bounds are large when $\min(\tilde{j}, \tilde{j}')$ is small, and $\mathbf{P}_K^{\text{sep}}$ decreases as $\min(\tilde{j}, \tilde{j}')$ increases. The maximum value of $\mathbf{P}_K^{\text{sep}}$ in these cases occur at $\{\tilde{j}, \tilde{j}'\} = \{1, K/2\}$.

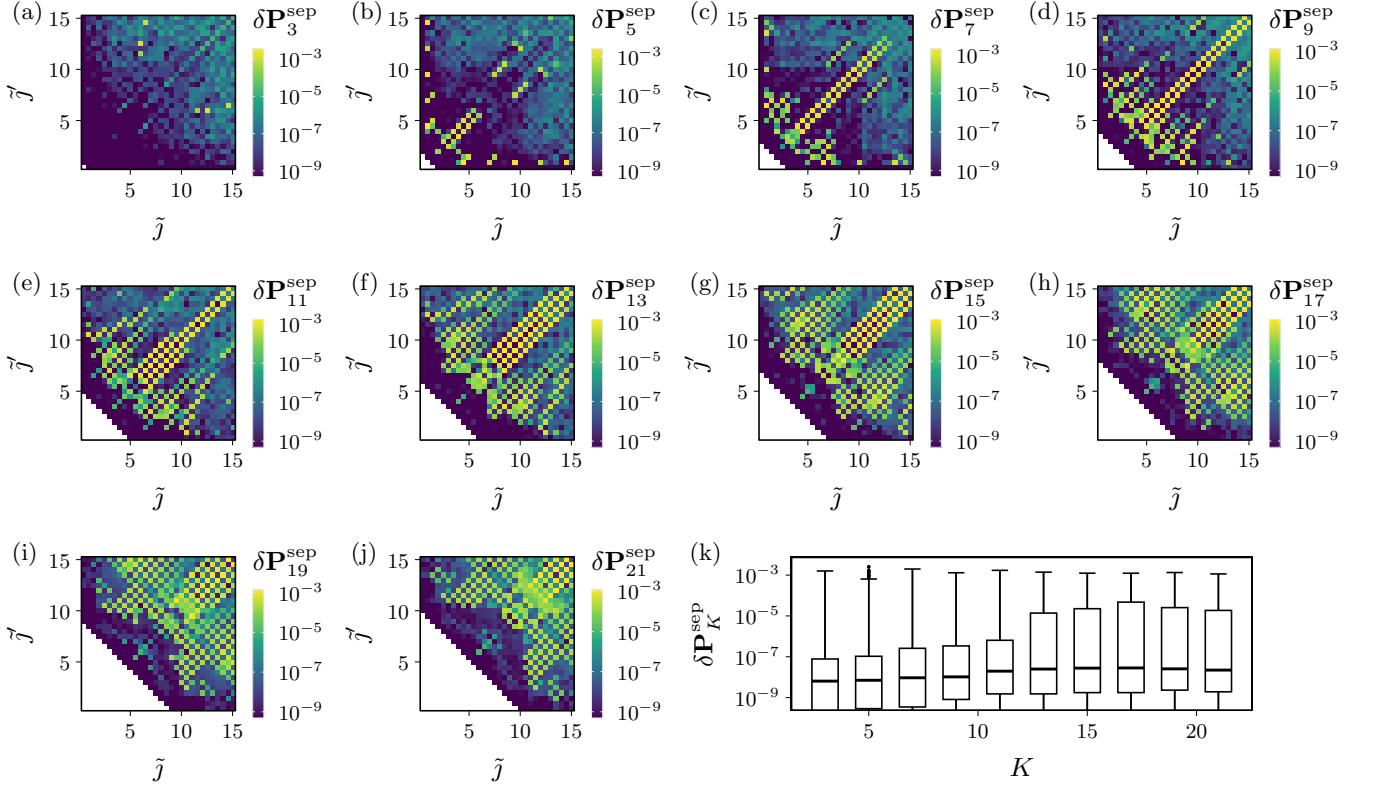


FIG. A2. (a)–(j) Heatmap of $\delta \mathbf{P}_K^{\text{sep}}(\{\tilde{j}, \tilde{j}'\})$, the deviations between the lower and upper bounds of $\mathbf{P}_K^{\text{sep}}$ computed using SPI and SDP, respectively, for different values of K . The errors are worse for large j as we used larger tolerances in those cases. This is because the value of $\mathbf{P}_K^{\text{sep}}$ is small, so the lower bounds for small j is larger than the upper bound of large j even with the larger tolerances for the latter. (k) Box plots of the errors against the number of measurements. The worst-case errors are of order 10^{-3} , but most lie within $\delta \mathbf{P}_K^{\text{sep}} \leq 10^{-5}$. Since the upper bound also includes positive-partial-transpose states (see Appendix D 2), this implies that bound-entangled states cannot be detected by our witness.

Appendix B: Key Technical Aspects of the Precession Protocol

We review some key technical aspects of the precession protocol used in this paper. For the full study with details and derivations, refer to Ref. [42].

Consider the protocol performed with a single fixed spin j such that the expected score for the state ρ given by $P_K = \text{tr}(\rho Q_K^{(j)})$, where

$$Q_K^{(j)} = \frac{1}{K} \sum_{k=0}^{K-1} \text{pos}(J_k^{(j)}) = \frac{1}{2} \left[\mathbb{1} + \frac{1}{K} \sum_{k=0}^{K-1} e^{-i(2\pi k/K)J_z^{(j)}/\hbar} \text{sgn}(J_x^{(j)}) e^{i(2\pi k/K)J_z^{(j)}/\hbar} \right]. \quad (\text{B1})$$

Here, $2 \text{pos}(J_k^{(j)}) |j, m\rangle_k = |j, m\rangle_k + \text{sgn}(m) |j, m\rangle_k$ and $J_k^{(j)} = e^{-i(2\pi k/K)J_z^{(j)}/\hbar} J_x^{(j)} e^{i(2\pi k/K)J_z^{(j)}/\hbar}$ were used. Some key properties of Q_K follow.

(1) $Q_K^{(j)}$ is block diagonal. Define the projector

$$\Pi_K^{(j, \bar{m})} := \sum_{k=0}^{\lfloor (j-\bar{m})/K \rfloor} |j, \bar{m} + kK\rangle \langle j, \bar{m} + kK|, \quad (\text{B2})$$

which projects onto the subspace of the eigenstates of $J_z^{(j)}$ whose eigenvalues are \bar{m} modulo K . Then, $Q_K^{(j)}$ has the block decomposition

$$Q_K^{(j)} = \frac{1}{2} \left[\mathbb{1} + \bigoplus_{\bar{m}=-j}^{\min(j, -j+K-1)} \Pi_K^{(j, \bar{m})} \text{sgn}(J_x^{(j)}) \Pi_K^{(j, \bar{m})} \right]. \quad (\text{B3})$$

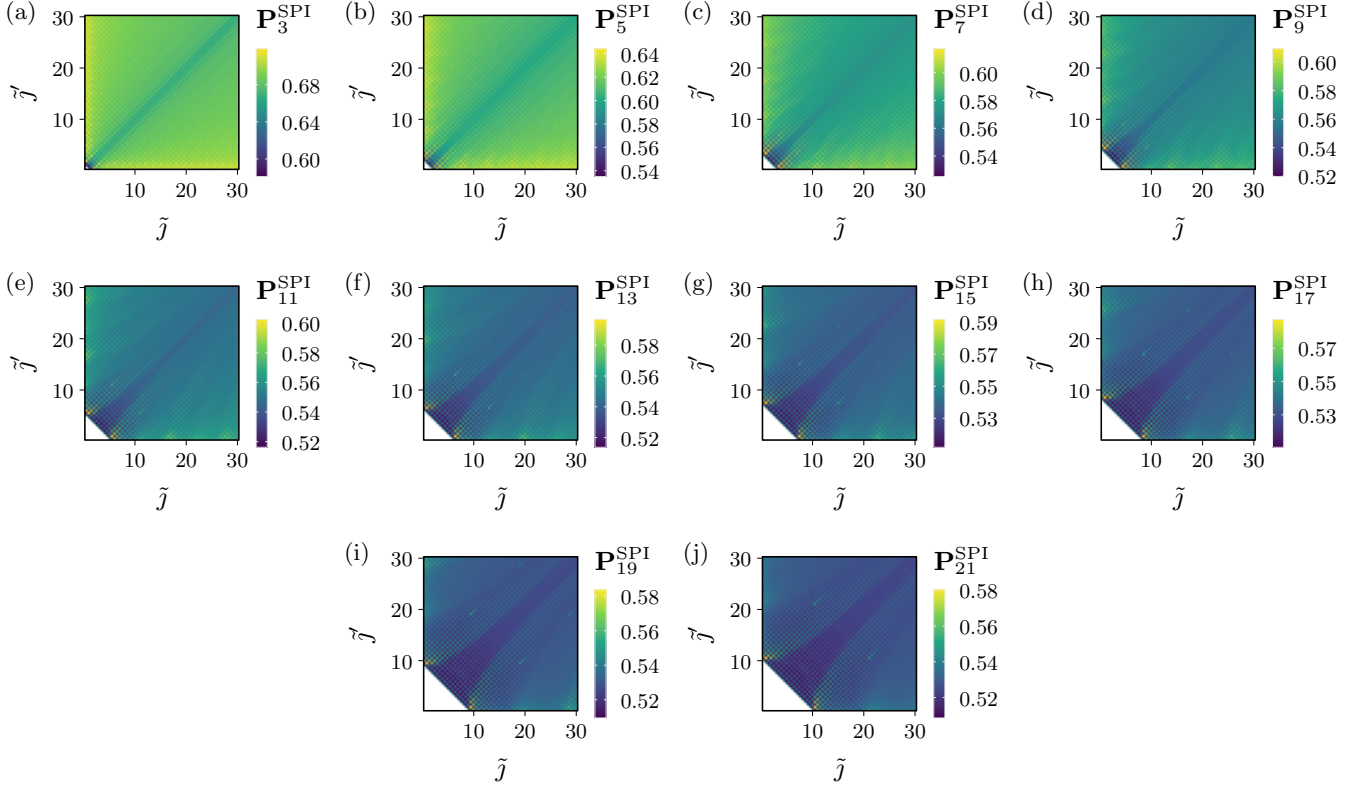


FIG. A3. Heatmap of $\mathbf{P}_K^{\text{SPI}}(\{\tilde{j}, \tilde{j}'\}) = \mathbf{P}_K^{\text{sep}}(\{\tilde{j}, \tilde{j}'\}) - \delta \mathbf{P}_K^{\text{sep}}(\{\tilde{j}, \tilde{j}'\})$, the lower bound of $\mathbf{P}_K^{\text{sep}}$, computed for larger values of \tilde{j} and \tilde{j}' . We were unable to compute the upper bounds for $\tilde{j}, \tilde{j}' > 15$ due to constraints of computational resources. However, from the small deviations between the upper and lower bounds for $\tilde{j}, \tilde{j}' \leq 15$ as seen in Fig. A2, we expect that $\mathbf{P}_K^{\text{SPI}}$ should also be rather close to the actual value $\mathbf{P}_K^{\text{sep}}$. We find that the behavior of $\mathbf{P}_K^{\text{SPI}}$ continues as expected, which is that it reduces in magnitude as \tilde{j} and \tilde{j}' increases, which lends further credence to Conjecture 3.

Consequently, if $j < K/2$, then $\bar{m} \leq K/2 - 1$ and hence $\lfloor (j - \bar{m})/K \rfloor = 0$, which implies that $2Q_K^{(j < K/2)} = \mathbb{1} + \sum_{m=-j}^j |j, m\rangle \langle j, m| \text{sgn}(J_x^{(j)}) |j, m\rangle \langle j, m|$ is diagonal with respect to the eigenstates of J_x .

(2) The matrix elements $\langle j, m | \text{sgn}(J_x^{(j)}) |j, m'\rangle$ are

$$\langle j, m | \text{sgn}(J_x^{(j)}) |j, m'\rangle = \begin{cases} 0 & \text{if } (m - m') \bmod 2 = 0, \\ \frac{(-1)^{(m' - m - 1)/2} 2^{-(2j-1)}}{m' - m} \sqrt{\frac{\binom{2\lfloor \frac{j+m}{2} \rfloor}{\lfloor \frac{j+m}{2} \rfloor} \binom{2\lfloor \frac{j-m}{2} \rfloor}{\lfloor \frac{j-m}{2} \rfloor}}{\binom{2\lfloor \frac{j+m'}{2} \rfloor}{\lfloor \frac{j+m'}{2} \rfloor} \binom{2\lfloor \frac{j-m'}{2} \rfloor}{\lfloor \frac{j-m'}{2} \rfloor}}} & \text{otherwise.} \\ \times \sqrt{\frac{(j+m)^{(j+m) \bmod 2} (j+m')^{(j+m') \bmod 2}}{(j-m)^{(j-m) \bmod 2} (j-m')^{(j-m') \bmod 2}}} & \end{cases} \quad (\text{B4})$$

In particular, the diagonal elements of $\text{sgn}(J_x^{(j)})$ are zero. From the previous result for $j < K/2$, we therefore have $2Q_K^{(j < K/2)} = \mathbb{1}_{(j < K/2)}$.

With the above two properties, $Q_K^{(j)}$ can be constructed for any given j , and its eigenvectors and eigenvalues can be found using standard numerical techniques. For some cases, this can even be done analytically. A special case we use in this paper is $K/2 \leq j < K$, where

$$\Pi_K^{(j, \bar{m})} \text{sgn}(J_x^{(j)}) \Pi_K^{(j, \bar{m})} = \begin{cases} 0 & \text{if } j + \bar{m} \leq \lfloor j - K/2 \rfloor, \\ \Psi_{+}^{(j, \bar{m})} \left(|\Psi_{+}^{(j, \bar{m})}\rangle \langle \Psi_{+}^{(j, \bar{m})}| - |\Psi_{-}^{(j, \bar{m})}\rangle \langle \Psi_{-}^{(j, \bar{m})}| \right) & \text{otherwise;} \end{cases} \quad (\text{B5})$$

with $\Psi^{(j,\bar{m})} = |\langle j, \bar{m} | \text{sgn}(J_x^{(j)}) | j, \bar{m} + K \rangle|$ and $|\Psi_{\pm\bar{m}}\rangle = (|j, \bar{m}\rangle \pm (-1)^{(K-1)/2} |j, \bar{m} + K\rangle) / \sqrt{2}$.

Appendix C: Separable Bound for $\{\bar{j}, \bar{j}'\} = \{1/2, (K+1)/2\}$

Given two spins with $\{j_1, j_2\} = \{1/2, (K+1)/2\}$, their total angular momentum can take values of $j \in \{K/2, K/2 + 1\}$. Therefore, defining $\Delta Q_K := \mathbb{1} - 2Q_K = \frac{1}{K} \sum_{k=0}^{K-1} \text{sgn}(J_k)$ for concision,

$$\begin{aligned} \Delta Q_K = & \left[\Pi_K^{(\frac{K}{2}, -\frac{K}{2})} \text{sgn}(J_x) \Pi_K^{(\frac{K}{2}, -\frac{K}{2})} \right] \oplus \left[\Pi_K^{(\frac{K}{2}+1, -\frac{K}{2})} \text{sgn}(J_x) \Pi_K^{(\frac{K}{2}+1, -\frac{K}{2})} \right] \\ & \oplus \left[\Pi_K^{(\frac{K}{2}+1, -\frac{K}{2}-1)} \text{sgn}(J_x) \Pi_K^{(\frac{K}{2}+1, -\frac{K}{2}-1)} \right] \oplus \left[\Pi_K^{(\frac{K}{2}+1, -\frac{K}{2}+1)} \text{sgn}(J_x) \Pi_K^{(\frac{K}{2}+1, -\frac{K}{2}+1)} \right]. \end{aligned} \quad (\text{C1})$$

With $\Pi_K^{(j,\bar{m})} \text{sgn}(J_x) \Pi_K^{(j,\bar{m})} = \Psi^{(j,\bar{m})} (|\Psi_+^{(j,\bar{m})}\rangle \langle \Psi_+^{(j,\bar{m})}| - |\Psi_-^{(j,\bar{m})}\rangle \langle \Psi_-^{(j,\bar{m})}|)$ from Eq. (B5) and direct computation of $\Psi^{(j,\bar{m})}$ from Eq. (B4), we obtain

$$\Psi^{(\frac{K}{2}, -\frac{K}{2})} = 2^{-(K-1)} \binom{K-1}{\frac{K-1}{2}}, \quad \Psi^{(\frac{K}{2}+1, -\frac{K}{2})} = \frac{\Psi^{(\frac{K}{2}, -\frac{K}{2})}}{K+1}, \quad \Psi^{(\frac{K}{2}+1, -\frac{K}{2} \mp 1)} = \sqrt{\frac{K+2}{2(K+1)}} \Psi^{(\frac{K}{2}, -\frac{K}{2})}. \quad (\text{C2})$$

We are interested in finding the separable bound

$$\begin{aligned} \mathbf{P}_K^{\text{sep}}(\{j_1, j_2\}) &= \max_{|\psi_{j_1}\rangle, |\psi_{j_2}\rangle} (\langle \psi_{j_1} | \otimes \langle \psi_{j_2} |) Q_K (| \psi_{j_1} \rangle \otimes | \psi_{j_2} \rangle) \\ &= \frac{1}{2} + \frac{1}{2} \max_{|\psi_{j_1}\rangle} \left\{ \max_{|\psi_{j_2}\rangle} \left[(\langle \psi_{j_1} | \otimes \mathbb{1}^{(j_2)}) \Delta Q_K (| \psi_{j_1} \rangle \otimes \mathbb{1}^{(j_2)}) \right] | \psi_{j_2} \rangle \right\}. \end{aligned} \quad (\text{C3})$$

By rewriting it as above, the maximization can be thought of as a two-step process: we first find the maximum eigenvalue of $(\langle \psi_{j_1} | \otimes \mathbb{1}^{(j_2)}) \Delta Q_K (| \psi_{j_1} \rangle \otimes \mathbb{1}^{(j_2)})$ for a fixed $|\psi_{j_1}\rangle$, then maximize this eigenvalue over all states $|\psi_{j_1}\rangle$. Parameterizing a generic state in $\mathcal{H}^{(j_1)}$ as $|\psi_{j_1}\rangle := \cos(\frac{\theta}{2}) |\frac{1}{2}, -\frac{1}{2}\rangle + e^{i\phi} \sin(\frac{\theta}{2}) |\frac{1}{2}, \frac{1}{2}\rangle$, and using the Clebsch–Gordan coefficients, we find

$$\begin{aligned} (\langle \psi_{j_1} | \otimes \mathbb{1}^{(j_2)}) | \Psi_{\pm}^{(\frac{K}{2}, -\frac{K}{2})} \rangle &= \cos\left(\frac{\theta}{2}\right) \sqrt{\frac{K+1}{2(K+2)}} | \frac{K+1}{2}, -\frac{K+1}{2} \rangle - \frac{e^{-i\phi} \sin(\frac{\theta}{2})}{\sqrt{2(K+2)}} | \frac{K+1}{2}, -\frac{K-1}{2} \rangle \\ &\pm (-1)^{\frac{K-1}{2}} \left(\frac{\cos(\frac{\theta}{2})}{\sqrt{2(K+2)}} | \frac{K+1}{2}, \frac{K-1}{2} \rangle - e^{-i\phi} \sin\left(\frac{\theta}{2}\right) \sqrt{\frac{K+1}{2(K+2)}} | \frac{K+1}{2}, \frac{K+1}{2} \rangle \right), \end{aligned} \quad (\text{C4a})$$

$$\begin{aligned} (\langle \psi_{j_1} | \otimes \mathbb{1}^{(j_2)}) | \Psi_{\pm}^{(\frac{K}{2}+1, -\frac{K}{2})} \rangle &= \frac{\cos(\frac{\theta}{2})}{\sqrt{2(K+2)}} | \frac{K+1}{2}, \frac{K+1}{2} \rangle + e^{-i\phi} \sin\left(\frac{\theta}{2}\right) \sqrt{\frac{K+1}{2(K+2)}} | \frac{K+1}{2}, \frac{K-1}{2} \rangle \\ &\pm (-1)^{\frac{K-1}{2}} \left(\cos\left(\frac{\theta}{2}\right) \sqrt{\frac{K+1}{2(K+2)}} | \frac{K+1}{2}, -\frac{K-1}{2} \rangle + \frac{e^{-i\phi} \sin(\frac{\theta}{2})}{\sqrt{2(K+2)}} | \frac{K+1}{2}, -\frac{K+1}{2} \rangle \right), \end{aligned} \quad (\text{C4b})$$

$$\begin{aligned} (\langle \psi_{j_1} | \otimes \mathbb{1}^{(j_2)}) | \Psi_{\pm}^{(\frac{K}{2}+1, -\frac{K}{2}-1)} \rangle &= \cos\left(\frac{\theta}{2}\right) \sqrt{\frac{K}{2(K+2)}} | \frac{K+1}{2}, \frac{K-3}{2} \rangle + \frac{e^{-i\phi} \sin(\frac{\theta}{2})}{\sqrt{K+2}} | \frac{K+1}{2}, \frac{K-1}{2} \rangle \\ &\pm (-1)^{\frac{K-1}{2}} \frac{e^{-i\phi} \sin(\frac{\theta}{2})}{\sqrt{2}} | \frac{K+1}{2}, -\frac{K+1}{2} \rangle, \end{aligned} \quad (\text{C4c})$$

$$\begin{aligned} (\langle \psi_{j_1} | \otimes \mathbb{1}^{(j_2)}) | \Psi_{\pm}^{(\frac{K}{2}+1, -\frac{K}{2}+1)} \rangle &= \frac{\cos(\frac{\theta}{2})}{\sqrt{K+2}} | \frac{K+1}{2}, -\frac{K-1}{2} \rangle + e^{-i\phi} \sin\left(\frac{\theta}{2}\right) \sqrt{\frac{K}{2(K+2)}} | \frac{K+1}{2}, -\frac{K-3}{2} \rangle \\ &\pm (-1)^{\frac{K-1}{2}} \frac{\cos(\frac{\theta}{2})}{\sqrt{2}} | \frac{K+1}{2}, \frac{K+1}{2} \rangle. \end{aligned} \quad (\text{C4d})$$

Notice therefore that $(\langle \psi_{j_1} | \otimes \mathbb{1}^{(j_2)}) \Delta Q_K (| \psi_{j_1} \rangle \otimes \mathbb{1}^{(j_2)})$ has support only in the subspace spanned by $\{ | \frac{K+1}{2}, -\frac{K+1}{2} \rangle, | \frac{K+1}{2}, -\frac{K-1}{2} \rangle, | \frac{K+1}{2}, -\frac{K-3}{2} \rangle, | \frac{K+1}{2}, \frac{K-3}{2} \rangle, | \frac{K+1}{2}, \frac{K-1}{2} \rangle, | \frac{K+1}{2}, \frac{K+1}{2} \rangle \}$. For $K > 3$, in this six-dimensional subspace,

$$\frac{(\langle \psi_{j_1} | \otimes \mathbb{1}^{(j_2)}) \Delta Q_K (| \psi_{j_1} \rangle \otimes \mathbb{1}^{(j_2)})}{\Psi(\frac{K}{2}, -\frac{K}{2})} \hat{=} \sqrt{\frac{K/2}{K+1}} \begin{pmatrix} 0 & 0 & 0 & e^{-i\phi} \sin(\theta) & 1 & -\sqrt{\frac{K/2}{K+1}} e^{i\phi} \sin(\theta) \\ 0 & 0 & 0 & 0 & 0 & 1 \\ 0 & 0 & 0 & 0 & 0 & e^{-i\phi} \sin(\theta) \\ e^{i\phi} \sin(\theta) & 0 & 0 & 0 & 0 & 0 \\ 1 & 0 & 0 & 0 & 0 & 0 \\ -\sqrt{\frac{K/2}{K+1}} e^{i\phi} \sin(\theta) & 1 & e^{i\phi} \sin(\theta) & 0 & 0 & 0 \end{pmatrix}. \quad (\text{C5})$$

This matrix is highly sparse, and its eigenvalues can be found by directly solving the characteristic equation $\det[(\langle \psi_{j_1} | \otimes \mathbb{1}^{(j_2)}) \Delta Q_K (| \psi_{j_1} \rangle \otimes \mathbb{1}^{(j_2)}) - \lambda \mathbb{1}] = 0$, which is given by

$$\left(\frac{\lambda}{\Psi(\frac{K}{2}, -\frac{K}{2})} \right)^2 \left\{ \left(\frac{\lambda}{\Psi(\frac{K}{2}, -\frac{K}{2})} \right)^4 (K+1)^2 - \left(\frac{\lambda}{\Psi(\frac{K}{2}, -\frac{K}{2})} \right)^2 \left[\frac{2K+1}{4} K \sin^2(\theta) + 2(K+1) \right] + \left(\frac{K \sin^2(\theta)}{8} + 1 \right)^2 \right\} = 0. \quad (\text{C6})$$

Removing the $\lambda = 0$ solutions, this equation is quadratic in λ^2 , with the solutions

$$\left(\frac{\lambda(\theta)}{\Psi(\frac{K}{2}, -\frac{K}{2})} \right)^2 = \left(\frac{K \sin(\theta) \pm \sqrt{(3K+1)K \sin^2(\theta) + 16(K+1)}}{4(K+1)} \right)^2. \quad (\text{C7})$$

Among the four solutions for $\lambda(\theta)$, whose dependence on $| \psi_{j_1} \rangle$ that is present through θ is now made explicit, we clearly have

$$\frac{\lambda_{\max}(\theta)}{\Psi(\frac{K}{2}, -\frac{K}{2})} = \frac{K |\sin(\theta)| + \sqrt{(3K+1)K \sin^2(\theta) + 16(K+1)}}{4(K+1)}. \quad (\text{C8})$$

To maximize this over θ , we only need to consider the range $\theta \in [0, \pi/2]$, as $\lambda_{\max}(\theta)$ repeats outside this range. Furthermore, since $\lambda_{\max}(\theta)$ is monotonically increasing with θ in this range, we arrive at

$$\max_{\theta} \lambda_{\max}(\theta) = \frac{2^{-(K+1)}}{K+1} \left(\frac{K-1}{\frac{K-1}{2}} \right) \left(K + \sqrt{3K^2 + 18K + 16} \right). \quad (\text{C9})$$

Note that the above is true only for $K > 3$. When $K = 3$, $\frac{K-3}{2} = -\frac{K-3}{2} = 0$, so the subspace is only five-dimensional. Nonetheless, repeating the above steps lead to a similar characteristic equation quadratic in λ^2 , with

$$\max_{\theta} \lambda_{\max}(\theta) = \max_{\theta} \frac{3|\sin(\theta)| + \sqrt{57 \sin^2(\theta) + 64}}{32} = \frac{7}{16}. \quad (\text{C10})$$

As such, recalling that $\max_{\theta} \lambda_{\max}(\theta)$ is the separability bound for ΔQ_K and $Q_K = (\mathbb{1} + \Delta Q_K)/2$, we arrive at

$$\mathbf{P}_K^{\text{sep}} \left(\left\{ \frac{1}{2}, \frac{K+1}{2} \right\} \right) = \frac{1}{2} (1 + \lambda_K), \quad \text{where} \quad \lambda_K = \begin{cases} \frac{7}{16} & \text{if } K = 3, \\ \frac{2^{-(K+1)}}{K+1} \left(\frac{K-1}{\frac{K-1}{2}} \right) \left(K + \sqrt{3K^2 + 18K + 16} \right) & \text{otherwise.} \end{cases} \quad (\text{C11})$$

Appendix D: Numerical Methods

Two numerical methods were used to find the lower and upper bounds of $\mathbf{P}_K^{\text{sep}}(\{j_1, j_2\})$ for general j_1, j_2 , which allows us to obtain reliable values of the separa-

ble bound to within numerical precision. We use a variant of the separability power iteration (SPI) [6] to obtain a lower bound $\mathbf{P}_K^{\text{SPI}}$, and semidefinite programming (SDP) [49] to obtain an upper bound $\mathbf{P}_K^{\text{SDP}}$. Note that the methods, while numerical, return reliable lower

and upper bounds, respectively. The scripts used and generated data are available in Ref. [52], while the implementation details of these two numerical techniques will be covered in the following sections.

After obtaining the two values, we can further define $\mathbf{P}_K^{\text{sep}} := (\mathbf{P}_K^{\text{SDP}} + \mathbf{P}_K^{\text{SPI}})/2$ and $\delta\mathbf{P}_K^{\text{sep}} := (\mathbf{P}_K^{\text{SDP}} - \mathbf{P}_K^{\text{SPI}})/2$. It is guaranteed that the actual value of the separability bound lies within the range $[\mathbf{P}_K^{\text{sep}} - \delta\mathbf{P}_K^{\text{sep}}, \mathbf{P}_K^{\text{sep}} + \delta\mathbf{P}_K^{\text{sep}}]$: henceforth, we will treat $\mathbf{P}_K^{\text{sep}}$ as an estimate for the true value of the separable bound, while $\delta\mathbf{P}_K^{\text{sep}}$ will be treated as a numerical error due to numerical precision and possible gaps between the two bounds.

For all studied cases, the gaps between the results obtained through these two numerical methods are small, where the largest deviation is of the order $\delta\mathbf{P}_K^{\text{sep}} \sim 10^{-3}$. These deviations are plotted for odd $K \leq 21$ in Fig. A2.

1. Lower Bounds: Separability Power Iteration

The lower bound can be found by noticing that $\mathbf{P}_K^{\text{sep}}(\{j_1, j_2\})$ is the global maximum of the product numerical range $\{\langle \psi_{j_1}, \psi_{j_2} | Q_K | \psi_{j_1}, \psi_{j_2} \rangle : |\psi_{j_1}, \psi_{j_2}\rangle = |\psi_{j_1}\rangle \otimes |\psi_{j_2}\rangle, |\psi_j\rangle \in \mathcal{H}^{(j)}\}$. As such, any particular choice of $|\psi_{j_1}, \psi_{j_2}\rangle$ must necessarily give a lower bound $\langle \psi_{j_1}, \psi_{j_2} | Q_K | \psi_{j_1}, \psi_{j_2} \rangle \leq \mathbf{P}_K^{\text{sep}}(\{j_1, j_2\})$.

By maximizing $\langle \psi_{j_1}, \psi_{j_2} | Q_K | \psi_{j_1}, \psi_{j_2} \rangle$ over $|\psi_{j_1}, \psi_{j_2}\rangle$ using any method, even if only a local maximum is reached, we can still obtain a lower bound that is as large as possible. As mentioned, we use a variant of the separability power iteration (SPI) [6] to obtain the lower bound $\mathbf{P}_K^{\text{SPI}}$. We detail the technique in Algorithm 1.

Algorithm 1 Bipartite variant of SPI

Require: $|a_0\rangle \in \mathcal{H}^{(j_1)}$, $0 < \varepsilon$

$p_{\text{prev}} \leftarrow -\infty$
 $p_{\text{curr}} \leftarrow \infty$
 $|a\rangle \leftarrow |a_0\rangle$
 $|b\rangle \leftarrow |b_0\rangle \in \mathcal{H}^{(j_2)} \triangleright \text{Any } |b_0\rangle \in \mathcal{H}^{(j_2)} \text{ will do}$
while $|p_{\text{curr}} - p_{\text{prev}}| \geq \varepsilon$ **do**

$|b\rangle \leftarrow \text{argmax}_{|\tilde{b}\rangle \in \mathcal{H}^{(j_2)}} \langle \tilde{b} | \text{tr}_{j_1} [Q_K (|a\rangle\langle a| \otimes \mathbb{1}^{(j_2)})] | \tilde{b}\rangle$
 $|a\rangle \leftarrow \text{argmax}_{|\tilde{a}\rangle \in \mathcal{H}^{(j_1)}} \langle \tilde{a} | \text{tr}_{j_2} [Q_K (\mathbb{1}^{(j_1)} \otimes |b\rangle\langle b|)] | \tilde{a}\rangle$
 $p_{\text{prev}} \leftarrow p_{\text{curr}}$
 $p_{\text{curr}} \leftarrow \langle a, b | Q_K | a, b \rangle$

return p_{curr}

Here tr_{j_n} is the partial trace over $\mathcal{H}^{(j_n)}$, while the steps requiring argmax are eigenvalue problems that can be solved with standard numerical libraries.

Algorithm 1 halts when the convergence condition $|p_{\text{curr}} - p_{\text{prev}}| < \varepsilon$ for a target precision ε is met. It can be shown that the algorithm is always convergent, and returns a local maximum for the given starting vector $|a_0\rangle \in \mathcal{H}^{(j_1)}$. Denote the vectors obtained in the n th round of Algorithm 1 by $|a_i\rangle$ and $|b_i\rangle$, and let

$p_i = \langle a_i, b_i | Q_K | a_i, b_i \rangle$. Then,

$$\begin{aligned} p_{i+1} &= \langle a_{i+1}, b_{i+1} | Q_K | a_{i+1}, b_{i+1} \rangle \\ &= \langle a_{i+1} | \text{tr}_{j_2} [Q_K (\mathbb{1}^{(j_1)} \otimes |b_{i+1}\rangle\langle b_{i+1}|)] | a_{i+1} \rangle \\ &\geq \langle a_i | \text{tr}_{j_2} [Q_K (\mathbb{1}^{(j_1)} \otimes |b_{i+1}\rangle\langle b_{i+1}|)] | a_i \rangle \quad (\text{D1}) \\ &= \langle b_{i+1} | \text{tr}_{j_1} [Q_K (|a_i\rangle\langle a_i| \otimes \mathbb{1}^{(j_2)})] | b_{i+1} \rangle \\ &\geq \langle a_i, b_i | Q_K | a_i, b_i \rangle = p_i \end{aligned}$$

This proves that $\{p_i\}_{i \geq 0}$ is monotonically increasing. Moreover, since Q_K is an observable that describes a probability and is therefore bounded from above, the sequence $\{p_i\}_{i \geq 0}$, which is a sequence of expectations of Q_K , is also bounded. Therefore, the monotonic sequence $\{p_i\}_{i \geq 0}$ converges, and hence Algorithm 1 will eventually halt for any starting vector $|a_0\rangle \in \mathcal{H}^{(j_1)}$.

Since the local maximum p we obtain depends on our choice of $|a_0\rangle$, we perform the algorithm with many different starting vectors $\{|a_0\rangle, |a'_0\rangle, |a''_0\rangle, \dots\}$ to obtain a set of local maximums $\{p, p', p'', \dots\}$. Following Ref. [6], we chose $\{|a_0\rangle, |a'_0\rangle, |a''_0\rangle, \dots\}$ to be the eigenvectors of generalized Gell-Mann matrices of dimension $2j_1 + 1$, which spans the full operator space in $\mathcal{H}^{(j_1)}$. Finally, we define $\mathbf{P}_K^{\text{SPI}} := \max\{p, p', p'', \dots\}$, which provides us with the best lower bound $\mathbf{P}_K^{\text{SPI}} \leq \mathbf{P}_K^{\text{sep}}$ that was found from the many runs of the algorithm.

2. Upper Bounds: Semi-Definite Programming

The upper bound is due to the Peres–Horodecki criterion, which states that the set of separable states $\{\rho_{\text{SEP}} : \rho_{\text{SEP}} = \sum_k p_k \rho_{j_1, k} \otimes \rho_{j_2, k}\}$ is a subset of the set of positive-partial-transpose states $\{\rho_{\text{PPT}} : \rho_{\text{PPT}}^{\Gamma_2} \succeq 0\}$ [60, 61]. Here, $\rho_{\text{PPT}}^{\Gamma_2}$ is the partial transposition of ρ_{PPT} whose matrix elements satisfy

$$\langle \psi_{j_1}, \psi_{j_2} | \rho_{\text{PPT}}^{\Gamma_2} | \phi_{j_1}, \phi_{j_2} \rangle = \langle \psi_{j_1}, \phi_{j_2} | \rho_{\text{PPT}} | \phi_{j_1}, \psi_{j_2} \rangle. \quad (\text{D2})$$

As $\mathbf{P}_K^{\text{sep}}$ involves a maximization over a subset of the positive-partial-transpose states, $\max_{\rho_{\text{PPT}}} \text{tr}(\rho_{\text{PPT}} Q_K)$ is an upper bound for $\mathbf{P}_K^{\text{sep}}$. Note that this would be a loose upper bound in general: there exists bound entangled states with positive partial transpose which are nonetheless inseparable [50, 51]. In turn, a reliable upper bound on $\max_{\rho_{\text{PPT}}} \text{tr}(\rho_{\text{PPT}} Q_K)$ can be obtained using semidefinite programming (SDP) [49], which we shall denote as $\mathbf{P}_K^{\text{SDP}}$. Being an upper bound of the upper bound for $\mathbf{P}_K^{\text{sep}}$, it is of course the case that $\mathbf{P}_K^{\text{SDP}} \geq \mathbf{P}_K^{\text{sep}}$.

Semidefinite programs are linear optimization problems of the form

$$\begin{aligned} &\max_{X \succeq 0} \text{tr}(CX) \\ &\text{subject to } \text{tr}(A_l X) = b_l \text{ for } l = 1, 2, \dots, \\ &X \succeq 0, \end{aligned} \quad (\text{D3})$$

where C and A_l are Hermitian operators. We refer to the above as the primal problem, and there is a related dual problem given by

$$\begin{aligned} \min_{y_1, y_2, \dots} \quad & \sum_l b_l y_l =: \vec{b} \cdot \vec{y} \\ \text{subject to} \quad & \sum_l y_l A_l \succeq C. \end{aligned} \quad (\text{D4})$$

The weak duality theorem states that the dual objective always upper bounds the primal one: that is, $\vec{b} \cdot \vec{y} \geq \text{tr}(CX)$. Weak duality therefore ensures that the global optimum of both the primal and dual problems are guaranteed to be between the gap given by the two objectives. As such, this is used as a convergence condition when numerically solving SDPs: local optimizations of the primal and dual problems are performed until $|\vec{b} \cdot \vec{y} - \text{tr}(CX)| < \varepsilon$ for a target precision ε .

For our purposes, we are interested in the optimization

$$\begin{aligned} \max_{\rho_{\text{PPT}}} \quad & \text{tr}(\rho_{\text{PPT}} Q_K) \\ \text{subject to} \quad & \rho_{\text{PPT}} \succeq 0 \\ & \rho_{\text{PPT}}^{\Gamma_2} \succeq 0. \end{aligned} \quad (\text{D5})$$

By setting $X = \rho_{\text{PPT}} \oplus \rho_{\text{PPT}}^{\Gamma_2}$, $C = Q_K \oplus 0$, and, for a Hermitian operator basis $\{O_l\}_l$ of $\mathcal{H}^{(j_1)} \otimes \mathcal{H}^{(j_2)}$, $A_l = O_l \oplus (-O_l^{\Gamma_2})$, Eq. (D5) can be rewritten into the form given in Eq. (D3). As such, our problem is an SDP, which can be solved by any SDP solver (we used JuMP [62] and COSMO [63] for the reported results). The objective value of the solution to the dual problem gives us a reliable upper bound $\mathbf{P}_K^{\text{SDP}} \geq \max_{\rho_{\text{PPT}}} \text{tr}(\rho_{\text{PPT}} Q_K) \geq \mathbf{P}_K^{\text{sep}}$.

Appendix E: Comparison to Other Criteria

In this appendix, we explicitly show that the states given as examples in Sec. IV E cannot be detected by other angular-momentum-based criteria. For reference, these are

$$\begin{aligned} |\text{GHZ}_K\rangle &= \frac{1}{\sqrt{2}} \left(\bigotimes_{n=1}^N |j_n, j_n\rangle + (-1)^{\frac{K-1}{2}} \bigotimes_{n=1}^N |j_n, -j_n\rangle \right), \\ |\Phi_5\rangle &= \frac{1}{2} \sqrt{\frac{7}{3}} \left(|\uparrow\rangle \otimes |\downarrow\rangle^{\otimes 6} - |\downarrow\rangle \otimes |\uparrow\rangle^{\otimes 6} \right) \\ &\quad - \frac{1}{2\sqrt{3}} (|D_1^7\rangle - |D_6^7\rangle), \\ |\Phi_3\rangle &= \frac{\sqrt{3}}{2} |\text{GHZ}_9\rangle - \frac{1}{2\sqrt{2}} (|D_3^9\rangle + |D_6^9\rangle). \end{aligned} \quad (\text{E1})$$

The subscript in the label denotes the number of measurements K with which to perform the precession protocol.

It can be verified that these example states are, by construction, eigenstates of $Q_K^{(j)}$, where $Q_K = \bigoplus_j Q_K^{(j)}$ and $Q_K^{(j)}$ acts on an irreducible subspace of $|\vec{J}\rangle^2$.

In the rest of this section, we will use $|\Psi_K\rangle \in \{|\text{GHZ}_K\rangle, |\Phi_3\rangle, |\Phi_5\rangle\}$ to discuss properties common to

all three states. As we will be discussing them in some generality, these discussions will also hold true for similar states with the same properties, for example, other simultaneous eigenstates of Q_K and $|\vec{J}\rangle^2$.

1. Some Properties of These Example States

To derive some general properties of $|\Psi_K\rangle$, we highlight two symmetries of Q_K : $e^{-i2\pi J_z/\hbar K} Q_K e^{i2\pi J_z/\hbar K} = Q_K$ and $e^{-i\pi J_x/\hbar} Q_K e^{i\pi J_x/\hbar} = Q_K$.

These can be verified with direct calculation, but also seen more intuitively: the chosen rotations applied on Q_K merely reshuffles, up to the modulus of T , the times $\{t_k\}_{k=0}^{K-1}$ over which the average of $\text{pos}(J_k)$ is calculated, which leaves Q_K invariant.

$$a. \quad \text{All example states have } \left\langle \sum_{j \in \mathbf{J}} \vec{J}^{(j)} \right\rangle = 0$$

From the previous discussion, we know that Q_K commutes with both $e^{i\pi J_x/\hbar}$, and therefore the two observables can be simultaneously diagonalized. Indeed, the given example states can be verified to also be eigenstates of $e^{-i\pi J_x/\hbar}$ with eigenvalues $\pm(-1)^j$.

This leads us to

$$\begin{aligned} \langle \Psi_K | J_z^{(j_n)} | \Psi_K \rangle &= \langle \Psi_K | e^{-i\pi J_x/\hbar} J_z^{(j_n)} e^{i\pi J_x/\hbar} | \Psi_K \rangle \\ &= -\langle \Psi_K | J_z^{(j_n)} | \Psi_K \rangle, \end{aligned} \quad (\text{E2})$$

which implies $\langle J_z^{(j_n)} \rangle = 0$, and hence $\langle \sum_{j \in \mathbf{J}} J_z^{(j)} \rangle = 0$.

Replacing $J_z \rightarrow J_y$ also gives $\langle \sum_{j \in \mathbf{J}} J_y^{(j)} \rangle = 0$.

Meanwhile, the commutation and hence simultaneous diagonalizability of Q_K and $e^{i2\pi J_z/\hbar K}$ similarly lets us choose the example states to be eigenstates of $e^{-i2\pi J_z/K}$ with eigenvalue $e^{-i2\pi m/K}$ for some m . Then, for any integer k ,

$$\begin{aligned} \langle \Psi_K | J_x^{(j_n)} | \Psi_K \rangle &= \langle \Psi_K | \left(e^{i2\pi J_z/K\hbar} \right)^k J_x^{(j_n)} \left(e^{-i2\pi J_z/K\hbar} \right)^k | \Psi_K \rangle \\ &= \cos\left(\frac{2\pi k}{K}\right) \langle J_x^{(j_n)} \rangle + \sin\left(\frac{2\pi k}{K}\right) \langle J_y^{(j_n)} \rangle. \end{aligned} \quad (\text{E3})$$

Taking the sum over $k \in \{0, 1, \dots, K-1\}$ and $j \in \mathbf{J}$ on both sides gives $\langle \sum_{j \in \mathbf{J}} J_x^{(j)} \rangle = 0$.

Since $e^{-i2\pi J_z/\hbar K}$ commutes with $J_z^{(j_n)}$, we also have

$$\begin{aligned} 0 &= \langle \Psi_K | J_z^{(j_{n-1})} J_x^{(j_n)} J_z^{(j_{n+1})} | \Psi_K \rangle \\ &= \langle \Psi_K | J_x^{(j_n)} J_z^{(j_{n+1})} | \Psi_K \rangle \\ &= \langle \Psi_K | J_z^{(j_{n-1})} J_x^{(j_n)} | \Psi_K \rangle \end{aligned} \quad (\text{E4})$$

for the example states.

Relatedly, with $e^{i2\pi J_z/\hbar K} J_\pm e^{-i2\pi/\hbar K} = e^{\mp i2\pi/K} J_\pm$ for $J_\pm := J_x \pm iJ_y$, similar steps imply

$$\langle \Psi_K | J_\pm^2 | \Psi_K \rangle = 0. \quad (\text{E5})$$

These properties will be useful in later sections.

b. Variances of total angular momentum of example states

The variance $(\Delta J_s)^2 := \langle J_s^2 \rangle - \langle J_s \rangle^2$ for $s \in \{x, y, z\}$ are all related to the quantity $\langle J_z^2 \rangle$ for these example states. Starting with $(\Delta J_s)^2 = \langle J_s^2 \rangle$ from $\langle J_s \rangle = 0$, and using $J_+ J_- + J_- J_+ = 2|\vec{J}|^2 - 2J_z^2$, we have

$$\begin{aligned} J_x^2 &= \frac{1}{4}(J_+ + J_-)^2 = \frac{1}{4}(J_+^2 + J_-^2 + 2|\vec{J}|^2 - 2J_z^2), \\ J_y^2 &= -\frac{1}{4}(J_+ - J_-)^2 = \frac{1}{4}(-J_+^2 - J_-^2 + 2|\vec{J}|^2 - 2J_z^2). \end{aligned} \quad (\text{E6})$$

Since $\langle J_\pm^2 \rangle = 0$, we end up with

$$\langle J_x^2 \rangle = \langle J_y^2 \rangle = \frac{1}{2} \langle |\vec{J}|^2 \rangle - \frac{1}{2} \langle J_z^2 \rangle \quad (\text{E7})$$

for these states.

2. Nondetection by Other Criteria

Given the above properties, we can now systematically apply each criteria to the example states.

a. Spin squeezing inequalities

Spin squeezing inequalities are GME witnesses that can be expressed in terms of the sum or product of variances of spin operators [35]. For a spin ensemble $\{j_n\}_{n=1}^N$, these inequalities take the general form

$$(\Delta u)^2 + (\Delta v)^2 \geq \hbar \min S_B, \quad (\text{E8})$$

$$\Delta u \Delta v \geq \frac{\hbar}{2} \min S_B, \quad (\text{E9})$$

where $u := \sum_{n=1}^N h_n J_x^{(j_n)}$, $v := \sum_{n=1}^N g_n J_y^{(j_n)}$, and h_n and g_n are real numbers. Meanwhile, the set S_B is defined as

$$\begin{aligned} S_B &:= \left\{ \left| \sum_{j_\alpha \in \mathbf{J}} h_\alpha g_\alpha \langle J_z^{(j_\alpha)} \rangle \right| + \left| \sum_{j_\beta \in \mathbf{J}^c} h_\beta g_\beta \langle J_z^{(j_\beta)} \rangle \right| \right. \\ &\quad \left. : \mathbf{J}-\mathbf{J}^c \text{ is a bipartition of } \{j_n\}_{n=1}^N \right\}. \end{aligned} \quad (\text{E10})$$

For the tripartite case, the authors also derived a spin version of an inequality first introduced for continuous variable systems [64]:

$$\min \left\{ \sum_{n=1}^3 B_n, \sum_{n=1}^3 S_n \right\} \geq \hbar \left| \sum_{n=1}^3 \langle J_z^{(j_n)} \rangle \right|, \quad (\text{E11})$$

where

$$\begin{aligned} B_n &:= \left[\Delta \left(J_y^{(j_{n'})} + J_y^{(j_{n''})} + g_n J_y^{(j_n)} \right) \right]^2 \\ &\quad + \left[\Delta \left(J_x^{(j_{n'})} - J_x^{(j_{n''})} \right) \right]^2, \end{aligned} \quad (\text{E12})$$

$$\begin{aligned} S_n &:= 2\Delta \left(J_y^{(j_{n'})} + J_y^{(j_{n''})} + g_n J_y^{(j_n)} \right) \\ &\quad \times \Delta \left(J_x^{(j_{n'})} - J_x^{(j_{n''})} \right), \end{aligned} \quad (\text{E13})$$

and (n, n', n'') is a permutation of $(1, 2, 3)$. Violating any of Eqs. (E8), (E9), or (E11) witnesses GME.

From Appendix E 1 a, we know that $\langle J_z^{(j_n)} \rangle = 0$ for all states in Eq. (E1), so all inequalities mentioned above become trivial, and no violation occurs. Hence, these inequalities cannot certify the GME of our example states.

Equation (E8) was later improved by replacing S_B on the right-hand side of the inequality with [36]

$$\begin{aligned} \tilde{S}_B &:= \left\{ \left| \sum_{j_\alpha \in \mathbf{J}} h_\alpha g_\alpha \langle J_z^{(j_\alpha)} \rangle \right| + \left| \sum_{j_\beta \in \mathbf{J}^c} h_\beta g_\beta \langle J_z^{(j_\beta)} \rangle \right| \right. \\ &\quad \left. + W_{\mathbf{J}, \mathbf{J}^c}^2 : \mathbf{J}-\mathbf{J}^c \text{ is a bipartition of } \{j_n\}_{n=1}^N \right\}, \end{aligned} \quad (\text{E14})$$

where

$$\begin{aligned} W_{\mathbf{J}, \mathbf{J}^c} &:= \sqrt{\Delta^2 u_{\mathbf{J}} + \Delta^2 v_{\mathbf{J}} - \left| \sum_{j_\alpha \in \mathbf{J}} h_\alpha g_\alpha \langle J_z^{(j_\alpha)} \rangle \right|^2} \\ &\quad - \sqrt{\Delta^2 u_{\mathbf{J}^c} + \Delta^2 v_{\mathbf{J}^c} - \left| \sum_{j_\beta \in \mathbf{J}^c} h_\beta g_\beta \langle J_z^{(j_\beta)} \rangle \right|^2} \end{aligned} \quad (\text{E15})$$

for $u_{\mathbf{J}} := \sum_{j_\alpha \in \mathbf{J}} h_\alpha J_x^{(j_\alpha)}$ and $v_{\mathbf{J}} := \sum_{j_\alpha \in \mathbf{J}} g_\alpha J_y^{(j_\alpha)}$, with $u_{\mathbf{J}^c}$ and $v_{\mathbf{J}^c}$ similarly defined. Again with $\langle J_z^{(j_n)} \rangle = 0$, the inequality becomes

$$\begin{aligned} &\langle (u_{\mathbf{J}} + u_{\mathbf{J}^c})^2 \rangle + \langle (v_{\mathbf{J}} + v_{\mathbf{J}^c})^2 \rangle \\ &\geq \left(\sqrt{\langle u_{\mathbf{J}}^2 \rangle + \langle v_{\mathbf{J}}^2 \rangle} - \sqrt{\langle u_{\mathbf{J}^c}^2 \rangle + \langle v_{\mathbf{J}^c}^2 \rangle} \right)^2, \end{aligned} \quad (\text{E16})$$

which is also trivially true, so the stronger form of this witness cannot detect the entanglement of the states under consideration.

b. Spin-half chain criterion

Another GME witness proposed for an N -partite spin-half chain involves the violation of the inequalities [17]

$$\left\langle \sum_{n=1}^N \tilde{\sigma}_x^{(j_n)} \right\rangle \leq \frac{N}{2}, \quad \sum_{n=1}^N \langle \tilde{\sigma}_x^{(j_n)} \rangle^2 \leq \frac{N}{2} \quad (\text{E17})$$

for $\tilde{\sigma}_x^{(j_n)} = \sigma_z^{(n-1)} \sigma_x^{(j_n)} \sigma_z^{(j_{n+1})}$ and $\sigma_z^{(j_0)} = \sigma_z^{j_{N+1}} = \mathbb{1}$,
 where $\sigma_s^{(j_n)} := 2J_s^{(j_n)}/\hbar$.

From Eq. (E4), $\langle \tilde{\sigma}_x^{(j_n)} \rangle = 0$ for all states under consideration, so the above inequalities are trivially satisfied. Therefore, they cannot be detected by these criteria.

c. Generalized spin squeezing inequalities

Generalized spin squeezing inequalities were first introduced for spin-half ensembles [19, 20], and later extended to larger spins [21, 22]. For an ensemble containing N spin- j particles, they take the form

$$D_1 = (\Delta J_x)^2 + (\Delta J_y)^2 + (\Delta J_z)^2 - N\hbar^2 j, \quad (\text{E18})$$

$$D_2^{(qrs)} = (N-1)(\tilde{\Delta} J_s)^2 - \left(\langle \tilde{J}_q^2 \rangle + \langle \tilde{J}_r^2 \rangle \right) + N(N-1)\hbar^2 j^2, \quad (\text{E19})$$

$$D_3^{(qrs)} = (N-1) \left[(\tilde{\Delta} J_q)^2 + (\tilde{\Delta} J_r)^2 \right] - \langle \tilde{J}_s^2 \rangle + N(N-1)\hbar^2 j^2, \quad (\text{E20})$$

where (q, r, s) is a permutation of (x, y, z) , and

$$\langle \tilde{J}_s^2 \rangle := \langle J_s^2 \rangle - \sum_{n=1}^N \left\langle \left(J_s^{(j_n)} \right)^2 \right\rangle = 2 \sum_{n \neq n'} \left\langle J_s^{(j_n)} J_s^{(j_{n'})} \right\rangle, \quad \left(\tilde{\Delta} J_s \right)^2 := \langle \tilde{J}_s^2 \rangle - \langle J_s \rangle^2. \quad (\text{E21})$$

Entanglement is certified by the negativity of any of the following quantities in Eqs. (E18) to (E20).

Since $\langle \vec{J} \rangle = 0$ for the example states, which gives $(\Delta J_s)^2 = J_s^2$ and $(\tilde{\Delta} J_k)^2 = \langle (\tilde{J}_k)^2 \rangle$, we have the simplification

$$D_1 = \langle J_x^2 \rangle + \langle J_y^2 \rangle + \langle J_z^2 \rangle - N\hbar^2 j = \langle |\vec{J}|^2 \rangle - N\hbar^2 j \quad (\text{E22})$$

$$\begin{aligned} D_2^{(qrs)} &= (N-1) \langle \tilde{J}_s^2 \rangle - \left(\langle \tilde{J}_q^2 \rangle + \langle \tilde{J}_r^2 \rangle \right) + N(N-1)\hbar^2 j^2 \\ &= N \langle \tilde{J}_s^2 \rangle + N(N-1)\hbar^2 j^2 - \sum_{r \in \{x, y, z\}} \langle \tilde{J}_r^2 \rangle \end{aligned} \quad (\text{E23})$$

$$\begin{aligned} &= N \langle \tilde{J}_s^2 \rangle + N(N-1)\hbar^2 j^2 - \langle |\vec{J}|^2 \rangle + \underbrace{\sum_{n=1}^N \langle |\vec{J}^{(j_n)}|^2 \rangle}_{N\hbar^2 j(j+1)} \\ &= N \langle \tilde{J}_s^2 \rangle + N\hbar^2 j(Nj+1) - \langle |\vec{J}|^2 \rangle, \end{aligned}$$

$$\begin{aligned} D_3^{(qrs)} &= (N-1) \left(\langle \tilde{J}_q^2 \rangle + \langle \tilde{J}_r^2 \rangle \right) - \langle \tilde{J}_s^2 \rangle + N(N-1)\hbar^2 j^2 \\ &= N \left(\langle \tilde{J}_q^2 \rangle + \langle \tilde{J}_r^2 \rangle \right) + N\hbar^2 j(Nj+1) - \langle |\vec{J}|^2 \rangle, \end{aligned} \quad (\text{E24})$$

which depends only on $\langle \tilde{J}_s^2 \rangle$ and $|\vec{J}|^2$. Using $|\vec{J}|^2 \leq N\hbar^2 j(Nj+1)$, we also have convenient lower bounds

$$D_2^{(qrs)} \geq N \langle \tilde{J}_s^2 \rangle, \quad D_3^{(qrs)} \geq N \left(\langle \tilde{J}_q^2 \rangle + \langle \tilde{J}_r^2 \rangle \right). \quad (\text{E25})$$

Hence, the nonnegativity of $\langle \tilde{J}_s^2 \rangle$ for all $s \in \{x, y, z\}$ is sufficient to imply the nonnegativity of $D_2^{(qrs)}$ and $D_3^{(qrs)}$.

We can now compute $D_2^{(qrs)}$ and $D_3^{(qrs)}$ for each of our example states. For the GHZ-like state defined in Eq. (E1), which for the N -partite spin- j chain is written as $|\text{GHZ}_K\rangle \propto |j, j\rangle^{\otimes N} + (-1)^{\frac{K-1}{2}} |j, -j\rangle^{\otimes N}$, we have

$$\begin{aligned} \langle \text{GHZ}_K | |\vec{J}|^2 | \text{GHZ}_K \rangle &= N\hbar^2 j(Nj+1) \\ \langle \text{GHZ}_K | \tilde{J}_s^2 | \text{GHZ}_K \rangle &= \sum_{\mu \in \{+j, -j\}} \left(\sum_{m \neq n} \langle j, \mu | J_s^{(j_m)} | j, \mu \rangle \langle j, \mu | J_s^{(j_n)} | j, \mu \rangle \right) \\ &= \begin{cases} 0, & \text{if } s \in \{x, y\} \\ N(N-1)\hbar^2 j^2 & \text{otherwise.} \end{cases} \end{aligned} \quad (\text{E26})$$

Since $\langle \text{GHZ}_K | |\tilde{J}|^2 | \text{GHZ}_K \rangle - N\hbar^2 j = N^2 \hbar^2 j^2 \geq 0$ and $\langle \text{GHZ}_K | \tilde{J}_s^2 | \text{GHZ}_K \rangle \geq 0$ for all s , none of the quantities in Eqs. (E18) to (E20) are negative.

We turn to the example states $|\Phi_5\rangle$ and $|\Phi_3\rangle$, which are states of an ensemble of seven and nine spin-half particles, respectively. Since $(J_s^{(j_n=1/2)})^2 = \hbar^2 \mathbb{1}/4$ for all s , we have $\sum_{n=1}^N \langle (J_s^{(j_n=1/2)})^2 \rangle = N\hbar^2/4$. Meanwhile, by direct computation, we also have

$$\langle \Phi_5 | |\tilde{J}|^2 | \Phi_5 \rangle = \frac{35}{4} \hbar^2, \quad \langle \Phi_5 | J_z^2 | \Phi_5 \rangle = \frac{25}{4} \hbar^2, \quad \langle \Phi_3 | |\tilde{J}|^2 | \Phi_3 \rangle = \frac{99}{4} \hbar^2, \quad \langle \Phi_3 | J_z^2 | \Phi_3 \rangle = \frac{63}{4} \hbar^2. \quad (\text{E27})$$

From this, we already have $\langle \Phi_5 | |\tilde{J}|^2 | \Phi_5 \rangle - 7\hbar^2/2 \geq 0$ and $\langle \Phi_3 | |\tilde{J}|^2 | \Phi_3 \rangle - 9\hbar^2/2 \geq 0$, hence $D_1 \geq 0$ for these two states. From Eq. (E7), we can further work out

$$\langle \Phi_5 | J_x^2 | \Phi_5 \rangle = \langle \Phi_5 | J_y^2 | \Phi_5 \rangle = \frac{\hbar^2}{2} \left(\frac{35}{4} - \frac{25}{4} \right) = \frac{5}{4} \hbar^2, \quad \langle \Phi_3 | J_x^2 | \Phi_3 \rangle = \langle \Phi_3 | J_y^2 | \Phi_3 \rangle = \frac{\hbar^2}{2} \left(\frac{99}{4} - \frac{63}{4} \right) = \frac{18}{4} \hbar^2. \quad (\text{E28})$$

This gives us

$$\langle \Phi_5 | \tilde{J}_s^2 | \Phi_5 \rangle = \begin{cases} -\frac{\hbar^2}{2} & \text{if } s \in \{x, y\} \\ \frac{9}{2} \hbar^2 & \text{otherwise,} \end{cases} \quad \langle \Phi_3 | \tilde{J}_s^2 | \Phi_3 \rangle = \begin{cases} \frac{11}{4} \hbar^2 & \text{if } s \in \{x, y\} \\ \frac{27}{2} \hbar^2 & \text{otherwise.} \end{cases} \quad (\text{E29})$$

Since $\langle \Phi_3 | \tilde{J}_s^2 | \Phi_3 \rangle \geq 0$, this already implies that the entanglement of $|\Phi_3\rangle$ cannot be witnessed by this criteria. For $|\Phi_5\rangle$, as $\langle \Phi_5 | \tilde{J}_z^2 | \Phi_5 \rangle \geq 0$ and $\langle \Phi_5 | \tilde{J}_z^2 | \Phi_5 \rangle + \langle \Phi_5 | \tilde{J}_s^2 | \Phi_5 \rangle \geq 0$ for $s \in \{x, y\}$, it is clear that $D_2^{(zxy)}$, $D_3^{(zxy)}$, and $D_3^{(yzx)}$ will be nonnegative. With further calculations, the other quantities can be found to be

$$D_2^{(xyz)} = D_2^{(yzx)} = \frac{7}{4} \hbar^2, \quad D_3^{(xyz)} = 0. \quad (\text{E30})$$

Therefore, none of the example states can be detected by the generalized spin inequalities.

d. Energy-based witnesses

For various spin models with a governing Hamiltonian H , the minimum energies E^{sep} achievable by separable states are known [24]. With that separable bound, a spin ensemble is detected to be entangled when $\langle H \rangle < E^{\text{sep}}$.

As an example, we consider two specific spin models from the cited paper. In both spin models, N spins are arranged on the vertices of a d -dimensional cubic lattice with periodic boundary conditions. Every spin pair connected by an edge is taken to be interacting.

Heisenberg lattice. For an anti-ferromagnetic Heisenberg Hamiltonian

$$H_H := \sum_{s \in \{x, y, z\}} \sum_{\langle j_n, j_i \rangle} \sigma_s^{(j_n)} \sigma_s^{(j_i)} + B \sum_{n=1}^N \sigma_z^{(j_n)}, \quad (\text{E31})$$

where $\langle j_n, j_i \rangle$ are interacting spin pairs and $\sigma_s^{(j_n)} := 2J_s^{(j_n)}/\hbar$, the separable bound for the energy is

$$E_H^{\text{sep}} = \begin{cases} -dN \left[\frac{1}{8} \left(\frac{B}{d} \right)^2 + 1 \right] & \text{if } \left| \frac{B}{d} \right| \leq 4, \\ -dN \left(\left| \frac{B}{d} \right| - 1 \right) & \text{otherwise.} \end{cases} \quad (\text{E32})$$

Meanwhile, since $\langle \vec{J} \rangle = 0$ implies $\langle \vec{\sigma} \rangle = 0$ for all example states, the last term of Eq. (E31) vanishes. Hence, we are only left with the $\sum_{\langle j_n, j_i \rangle} \langle \sigma_s^{(j_n)} \sigma_s^{(j_i)} \rangle$ terms.

For $|\text{GHZ}_K\rangle$ and $|\Phi_3\rangle$, notice that they are totally symmetric under any permutation of the individual spins. So, the expectation value $\langle \sigma_s^{(j_n)} \sigma_s^{(j_i)} \rangle$ is the same for all interacting spin pairs, and since there are Nd of them,

$$\sum_{\langle j_n, j_i \rangle} \langle \Psi_K | \sigma_s^{(j_n)} \sigma_s^{(j_i)} | \Psi_K \rangle = Nd \langle \Psi_K | \sigma_s^{(j_1)} \sigma_s^{(j_2)} | \Psi_K \rangle \quad (\text{E33})$$

for these two states.

Computing the expectation value $\langle \sigma_s^{(j_1)} \sigma_s^{(j_2)} \rangle$ gives us

$$\sum_{\langle j_n, j_i \rangle} \langle \text{GHZ}_K | \sigma_s^{(j_n)} \sigma_s^{(j_i)} | \text{GHZ}_K \rangle = \begin{cases} \frac{Nd}{2} & \text{if } s \in \{x, y\}, \\ 0 & \text{otherwise,} \end{cases} \quad (\text{E34})$$

$$\sum_{\langle j_n, j_i \rangle} \langle \Phi_3 | \sigma_s^{(j_n)} \sigma_s^{(j_i)} | \Phi_3 \rangle = \begin{cases} \frac{Nd}{8} & \text{if } s \in \{x, y\}, \\ \frac{3Nd}{4} & \text{otherwise.} \end{cases} \quad (\text{E35})$$

For the state $|\Phi_5\rangle$, since the only possible cubic lattice with seven spins is a spin chain, we only need to consider the $d = 1$ case. Direct computation gives

$$\sum_{\langle j_n, j_i \rangle} \langle \Phi_5 | \sigma_s^{(j_n)} \sigma_s^{(j_i)} | \Phi_5 \rangle = \begin{cases} -\frac{1}{3} & \text{if } s \in \{x, y\}, \\ 3 & \text{otherwise.} \end{cases} \quad (\text{E36})$$

The positivity of the energies for $|\text{GHZ}_K\rangle$ and $|\Phi_3\rangle$ is evident from Eqs. (E34) and (E35). Meanwhile, Eq. (E36)

also gives

$$\langle \Phi_5 | H_H | \Phi_5 \rangle = \frac{7}{3} > 0. \quad (\text{E37})$$

Therefore, since $E_H^{\text{sep}} < 0 < \langle \Psi_K | H_H | \Psi_K \rangle$, this method is unable to detect the entanglement of all example states.

XY model. For the XY Hamiltonian

$$H_{XY} := \sum_{s \in \{x, y\}} I_s \sum_{\langle n, l \rangle} \sigma_s^{(j_n)} \sigma_s^{(j_l)} + B \sum_{n=1}^N \sigma_z^{(k)}, \quad (\text{E38})$$

where $\langle j_n, j_l \rangle$ are interacting spin pairs and $\sigma_s^{(j_n)} := 2J_s^{(j_n)}/\hbar$, the separable bound for the energy is

$$E_{XY}^{\text{sep}} = \begin{cases} -dNI \left(1 + \frac{B^2}{4}\right) & \text{if } b \leq 2, \\ -dNIb & \text{otherwise,} \end{cases} \quad (\text{E39})$$

with $I = \max\{|I_x|, |I_y|\}$ and $b = |B|/(Id)$.

Similar to the case of the Heisenberg lattice, since $E_{XY}^{\text{sep}} < 0$, Eqs. (E34) and (E35) already rule out the possibility of detecting the entanglement of $|\text{GHZ}_K\rangle$ and $|\Phi_3\rangle$ using this method.

For the remaining state, Eq. (E36) gives

$$\langle \Phi_5 | H_{XY} | \Phi_5 \rangle = -\frac{1}{3}(I_x + I_y) \geq -\frac{2I}{3}. \quad (\text{E40})$$

As previously mentioned, the only cubic lattice configuration for seven spins is one-dimensional. Consequently, Eq. (E39) implies that $E_{XY}^{\text{sep}} \leq -7I < \langle \Phi_5 | H_{XY} | \Phi_5 \rangle$. Therefore, this method also fails to detect the entanglement of $|\Phi_5\rangle$.